Electrochromic Properties of Vanadium Pentoxide Nanostructured Thin Films

Afaf Almoabadi

A Thesis

In

The Department

Of

Physics

Presented in Partial Fulfillment of the Requirements

For the Degree of Master of Science in Physics at Concordia University

Montreal, Quebec, Canada

August 2015

CONCORDIA UNIVERSITY
School of Graduate Studies

This is to certify that the thesis prepared

By: Ms. Afaf Almoabadi

Entitled: Electrochromic Properties of Vanadium Pentoxide Nanostructured Thin Films

and submitted in partial fulfillment of the requirements for the degree of

Master of Science (Physics)

complies with the regulations of the University and meets the accepted standards with respect to originality and quality.

Signed by the final examining committee:

Prof. Laszlo Kalman Chair

Prof. Claudine Gauthier Examiner

Prof. Pablo Bianucci Examiner

Prof. Truong Vo-Van Supervisor

Approved by Prof. Alexandre Champagne
Chair of Department or Graduate Program Director

Prof. Andre Roy
Dean of Faculty

Date September 12, 2015

ABSTRACT

Electrochromic Properties of Vanadium Pentoxide Nanostructured Thin Films

Afaf Almoabadi

The focus of this work is the improvement of the electrochromic properties of vanadium pentoxide thin films in order to expand its use. Indeed, because of its rather poor electrochromic properties, until now, vanadium pentoxide has only been used as a storage material in an electrochromic device, in conjunction with tungsten oxide, molybdenum oxide etc. To this purpose, vanadium pentoxide thin films were prepared under different conditions and characterized by using optical and electrochemical methods. Films were deposited on indium tin oxide (ITO) substrates by dip-coating at both room- and sub-zero temperature (-10^0C) and porosity in the sol-gel prepared vanadium pentoxide film was created by using templating methods. The morphology, optical and electrochromic properties of the macro- and mesoporous films, prepared in the presence of structure-directing agents such as polystyrene microspheres and triblock copolymer, have been compared with those of dense films. By using various methods to remove the template material, it was shown that the morphology of the vanadium pentoxide film can be controlled and new nanostructures can be created. The transformation of the lamellar into a nanorod structure, observed when the film is heated at 425-500◦C for several hours, resulted in the development of an elegant method for the synthesis of vanadium oxide nanostructures. The electrochromic performance of the nanorods prepared through the thermal treatment was found to be superior to that of the vanadium pentoxide with the layered structure, especially in the near-infrared region, demonstrating their potential for electrochromic applications. The structure, morphology, optical and electrochromic properties of dense and porous vanadium oxide films, coated at low temperature were also determined and compared to those of the corresponding films, deposited under room-temperature conditions. The results indicated that in the films coated at -10^0C, a residual compressive stress exists that originates from a non-uniformity in depth of the film, most probably, due to the formation of micro voids during the deposition. The micro voids are preserved during the heat-treatment of the films. The

"micro void" morphology was found to account for the considerably improved electrochromic properties of the sub-zero dip-coated films. Low-temperature coated films, heated at 450^0C for several hours, undergo the transformation from a layered to a highly uniform nanorod structure with important potential optoelectronic applications. The overall aim of this work is thus to evaluate how the morphology of vanadium pentoxide thin films is instrumental in obtaining a material with a high lithium ion intercalation capacity. With an appropriate morphology, the performance of vanadium oxide as electrochromic material and as cathode in lithium ion batteries can be improved significantly. For this purpose, both layered (dense and porous) and nanorod films were prepared and characterized. Scanning electron microscopy, cyclic voltammetry and electrical impedance spectroscopy measurements were used for the characterization of the different V_2O_5 films.

Acknowledgments

Firstly, I would like to express my sincere gratitude to my advisor, Prof. Truong Vo-Van, for his continuous support of my MSc studies and related research, for his patience, motivation, and immense knowledge. His guidance helped me throughout both the research and writing of this thesis. I could not imagine having a better advisor and mentor for my MSc study.

Besides my advisor, I would like to thank the rest of my thesis committee: Prof. Claudine Gauthier and Prof. Pablo Bianucci for their insightful comments and encouragement.

My special thanks go to our group members Drs. Simona Badilescu, Mohammed Alsawafta, Victor Stancovski, Tanu Sharma and Ralf Brüning: I would like to thank Simona for her unflagging support and assistance in my work, and her friendship, which I value above all. Her interest and assistance in my work made me like we were more family than colleagues. I would like to thank Mohammed for helping me with the analysis of electrochromic devices and for giving me my initial training in the lab; I wish you the best in your job in Kuwait. I would like also to thank Victor for the EIS measurements and his support for my thesis. Of course, I would like to thank Tanu and Ralf for doing the XRD measurements and their support as well.

I would also like to thank to my undergraduate teachers Dr. Hala Al-Jawhari and Dr. Najwa Enaiah in the department of Physics in King Abdulaziz University in Jeddah. I would not have reached this goal without your support!

My sincere thanks also goes to my English teacher Katherine Cormier who helped me a lot for improving my English and taught me a great deal over the last five years.

I would also like to thank my family: my parents and my brothers, especially Ahmd Almoabdi, and my sisters, especially Fatima Almoabdi, for coming with me to Canada and supporting me spiritually throughout writing this thesis and my life in general. I could not have accomplished all of this without their support and encouragement.

Finally, I recognize that my masters degree would not have been possible without the financial support of the Ministry of Higher Education and the Saudi Arabian Cultural Bureau in Canada,

who organized my scholarship in Canada; thank you for choosing me for the scholarship program, funding my education and helping me build my future.

Table of Contents

List of Tables

List of Figures

Chapter 1

1 Introduction

Vanadium pentoxide gels can be used in energy storage/conversion devices such as electrochromic (EC) devices, rechargeable lithium ion battery technologies, and pseudocapacitor applications [1-3]. Other interesting applications encompass optical filters, reflectance mirrors, and surfaces with tunable emittance for temperature control of space vehicles [4]. Vanadium oxide is used as cathode material in lithium batteries [5], in bolometric detectors [6], and as ferromagnetic nanotubes [7-9]. Important examples are the use of vanadium oxide-based catalysts in the synthesis of bulk chemicals like SO_3, propene, etc., and in the reduction of environmental pollution, for example, the reduction of nitrogen oxides NO_x in the exhaust gas from power plants.

1.1 Background of present study

Vanadium oxide thin films, as many other transition metal oxides, have been prepared using physical techniques such as sputtering [10-12], thermal evaporation [13], pulse laser deposition [14], e-beam deposition [15], flash-evaporation [16], chemical vapor deposition [17] and spray pyrolysis [18].

The thermal evaporation and sputtering methods were among the first methods that were used for the fabrication and characterization of vanadium pentoxide films and they continue to be used today for specific applications. However, after the development of sol-gel route, many of the studies in the field of electrochromism (EC) were based on sol-gel methods because of the simplicity and the milder conditions.

Vanadium pentoxide showed good sensing and catalytic properties. However, the moderate electrical conductivity ($10^{-3} - 10^{-2}$ S.cm^{-1}) and quite low Li^+ diffusion coefficient in V_2O_5, are limiting the intercalation properties. For practical applications, an important goal is to achieve a large storage capacity, that is, to enhance lithium ion intercalation. One approach, developed recently, is by using templating methods in order to create porosity in the sol-gel prepared

vanadium pentoxide. Studies have thus focused on maximizing the electrolyte contact area and decreasing the Li-ion diffusion distance [19-21].

In addition, vanadium pentoxide xerogel films (hydrated metal oxide films formed through a sol-gel process) have a layered structure; ions and molecules can be easily intercalated between adjacent layers without changing its structural integrity. Ion insertion/extraction is facilitated by the large contact area with the electrolyte and small sizes of nanostructures. Using nanostructured vanadium pentoxide with various morphologies in EC devices is expected to enhance their characteristics because of the inherently high surface area to volume ratio and short diffusion paths that facilitate ion and electron transfer.

Among the different nanostructures for lithium intercalation applications, vanadium pentoxide nanotubes and nanorods have been found to be the most promising, especially as electrode material for lithium ion batteries [19].

Nanorod host matrices for lithium intercalation have been prepared by using a sol-gel method, in combination with adequate structure-directing molecules. The fabrication of vanadium oxide in a tubular form was first accomplished by Ajayan et al. in 1995 by using carbon nanotubes as templates. Later on, a new soft-chemistry (sol-gel) method was developed by Nesper et al. using vanadium oxide precursors and alkyl amines or α,ω-diamines with long alkyl chains as templates. Nanotubes were obtained in a high yield, after aging and a hydrothermal treatment [22–26]. They could be obtained from an ammonium metavanadate precursor as well, and a rolling mechanism for the formation of vanadium oxide nanotubes from lamellar structures has been described by Chen et al [27]. They have a scroll-type morphology and the vanadium oxide layers inside the walls have been found to be crystalline.

Vanadium oxide nanorods have been also synthesized by using a reverse micelle technique [28], and arrays were grown by electrochemical deposition [29]. Wang et al. reported an interesting method to transform the layered vanadium oxide thin films deposited on silicon wafer substrates into nanorods by heating them in air to 400–500◦C. They used a thermal oxidation method and the nanorods were formed without any template material [30].

Except for the work by Wang et al., all the above-mentioned methods were very tedious, using the hydrothermal treatment of a vanadium oxide precursor in the presence of a primary amine template. The synthesis was carried out in an autoclave at 160–180◦C for one week and led to the formation of both nanotubes and nanorods in the form of a powder product. Only Wang et al. reported on the preparation of vanadium pentoxide nanotubes and nanorods in the form of a thin film [30]. In this work, the preparation of the film on a Si substrate was carried out by electrodeposition, using a vanadium sheet. However, no data could be found in the literature on the electrochromic (EC) properties of nanotubular or nanorod structures. In order to investigate their performance, it is important to develop a simpler method to fabricate thin films to be used as electrodes in an EC device. It should be noted that the vanadium pentoxide nanostructures prepared by the above-described methods were found to be redox active, undergoing a reversible reaction with lithium ions. The large lithium insertion capacity found for vanadium pentoxideelectrode in lithium-ion batteries was associated to the different topological intercalation sites provided by the nanotubular or nanorod host structures and the shorter diffusion paths involved [1, 22–27].

It has been shown that length uniformity is of great importance in fabrication of nanorods and nanowires as building blocks for applications that involve electron and ion flow [31]. In addition, because of the large high aspect ratio, low dimensional nanostructures such as nanowires and nanorods, have many nanotips that make them interesting for field emission displays. For this application, the uniformity would be an asset as well [32].

1.2 Contribution of this work

Sol-gel synthesis has proven to be one of the most convenient methods to prepare electrochromic nanostructured vanadium pentoxide films. In the sol-gel technique, the deposition sol is prepared by the hydrolysis and condensation of a vanadium oxide precursor solution. The method is relatively simple and the concentration of reactants can be controlled accurately. There is today a plethora of precursor molecules both organic and inorganic, and, generally, the chemistry of the reactions is well known. The solutions can be easily coated on indium tin oxide (ITO) substrates by dip- and spin-coating, by using relatively simple equipment [33 – 39]. Kim et al. [40] recently

developed a new technique of dip-coating, termed "sol-gel synthesis at sub-zero temperatures", and used it for the deposition of zinc oxide thin films. They have studied the effect of the dip-coating temperature on the structure and optical properties of the films and have found that at sub-zero temperatures, the deposition rate is higher because of the higher viscosity of the solution.

In this work porous vanadium pentoxide films were prepared by using templating methods. It has been reported that templated sol-gel prepared vanadium oxide films yield, after removing the template, meso- (pores in the size range of 2 to 20 nm) or macro porous films with significantly enhanced electrochromic properties [41-51]. In order to create porosity in vanadium pentoxide xerogel prepared from a vanadium alkoxide, we have used polystyrene microspheres or a non-ionic polymer surfactant (Pluronic P-123) and heat-treated the dip-coated layers on indium tin oxide (ITO) substrates at relatively high temperatures (400–500◦C). Interestingly, the SEM images of the samples revealed the formation of nanorod structures, similar to those reported earlier [22–27]. The morphology, optical and electrochromic properties of the macro- and mesoporous films, prepared in the presence of structure-directing agents, have been compared with those of dense films [41]. The transformation of the lamellar into a nanorod structure, observed when the film is heated at 400–500°C for several hours, resulted in the development of an elegant method for the synthesis of vanadium oxide nanorods [41]. We intended to investigate this transformation under different conditions, by dip-coating the precursor solution at a low (sub-zero) temperature and to take advantage of the higher rate of deposition.

The present study examines the effect of meso- and macroporosity on the optical and electrochromic properties of sol-gel prepared vanadium oxide films. The formation of nanorods under different conditions is investigated in order to perfect a relatively simple method to synthesize vanadium oxide nanorod structures for EC applications. Vanadium pentoxide is prepared by the catalyzed hydrolysis and polycondensation of vanadium tr (isopropoxide)oxide in a 2-propanol solution in the presence of polystyrene microsphere or triblock copolymer template. Our discussion will be focused on the EC properties of the highly porous vanadium pentoxide thin films. The EC properties of the nanorod films are also compared to those of the layered sol-gel films.

The mechanism of the coloring/bleaching process determines the response time and the cycling stability of the electrochromic device. Understanding the mechanism of ion insertion into the EC film and its relation to the microstructure of the film is crucial for the fabrication of films having improved electrochromic properties and, consequently, better device performance.

Chapter 2

2 Experimental

The specific methodology used for the preparation and experimental set-up is presented in this chapter. The procedure for preparing the thin electrochromic films is based on the method of dip-coating.

First, the vanadium oxide precursor solution was prepared as described in detail in section 2.2 and then it was coated onto an ITO substrate and further the film was annealed.

2.1 Preparation of glass substrate

Indium tin oxide (ITO) has been used as the transparent conductive substrate. Indium tin oxide is coated on polished soda lime float glass. The resistance of the ITO substrate was about 15 Ω/sq. Figure (2.1) shows the visible and near-infrared regions of transmittance spectrum of the ITO-glass.

Once the substrates are dried after cleaning, they are tested with a multimeter to determine which side has the ITO. Then the non-ITO side is covered with scotch tape. This ensures that the coating solution will be applied only to the ITO side, resulting in more transparent substrates.

The large ITO-glass sheets were cut into smaller (4cm x 2cm) pieces, so that they could be utilized as substrates for the optical and electrochemical measurements. The substrates were thoroughly cleaned by following the procedure described below:

1) Laboratory soap, water and deionized water are used to clean and remove dust from both sides of the substrates.

2) Contaminants from both sides of the substrate as well as water were removed with acetone.

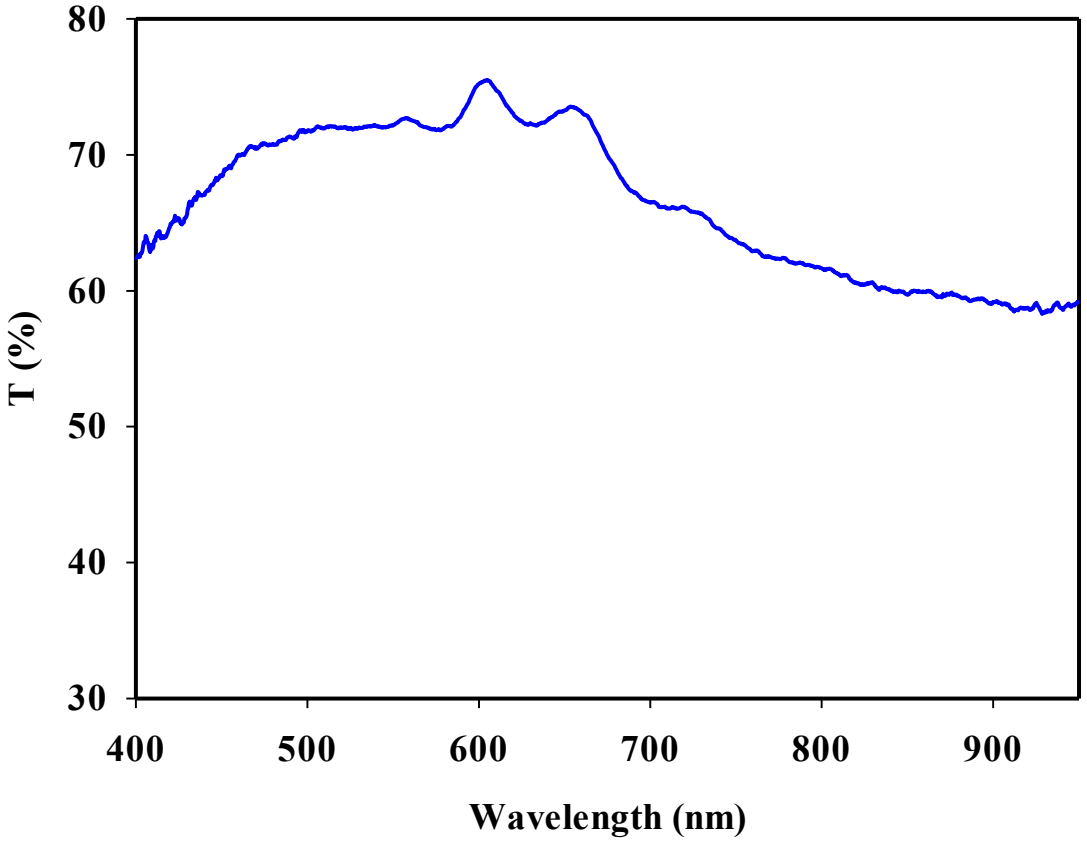

Figure 2.1: Visible and near-infrared spectrum of the indium tin oxide (ITO)-glass

3) Acetone was removed with isopropyl alcohol (IPA).

4) Samples were left to dry vertically.

2.2 Preparation of the coating solution

The preparation of the coating solution is described in the flow chart shown in Figure (2.2). The coating solution was prepared according to reference [52]. The reaction of hydrolysis of the vanadium alkoxide that leads to the formation of hydroxyl bonds can be written as:

$$(C_3H_7O)_2\ OV(OC_3H_7) + H_2O \rightarrow (OC_3H_7)_2OV(OH) + C_3H_7OH \quad (1)$$

Further, the reaction of the hydroxyl groups with the alkoxy groups of the neighboring molecules leads to the formation of the vanadium oxide network:

$(C_3H_7O)_2\,OV(OH) + (C_3H_7O)VO(OC_3H_7)_2 \rightarrow = (OV - O - VO) + C_3H_7\,OH$…… (2)

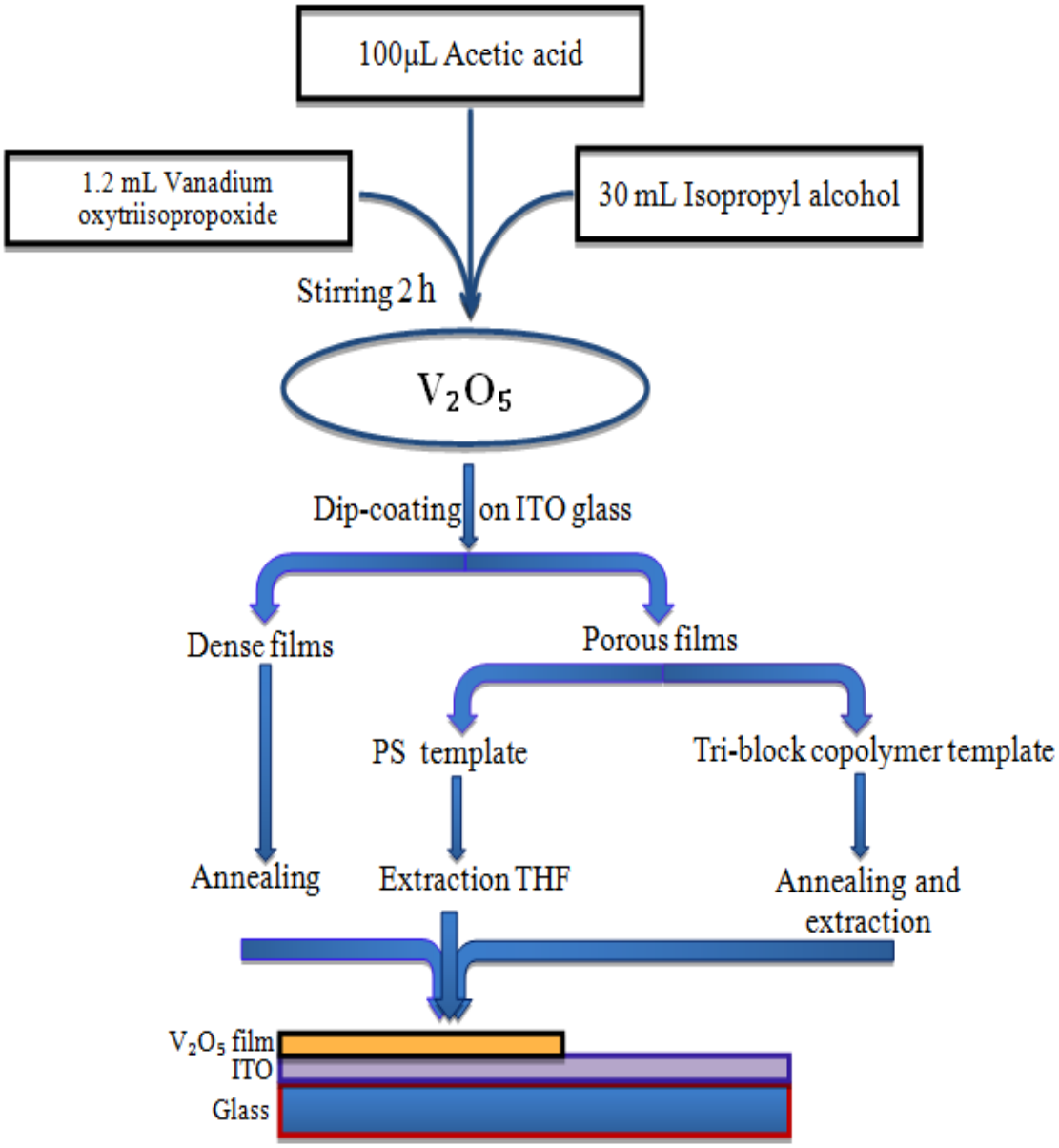

Figure 2.2: Flow-chart showing the fabrication of V_2O_5 xerogel and the porous films

The synthesis is carried out in an open beaker; therefore, the hydrolysis does not need additional water. After 2 hours of stirring, a transparent, yellow-orange solution was obtained and used for dip-coating.

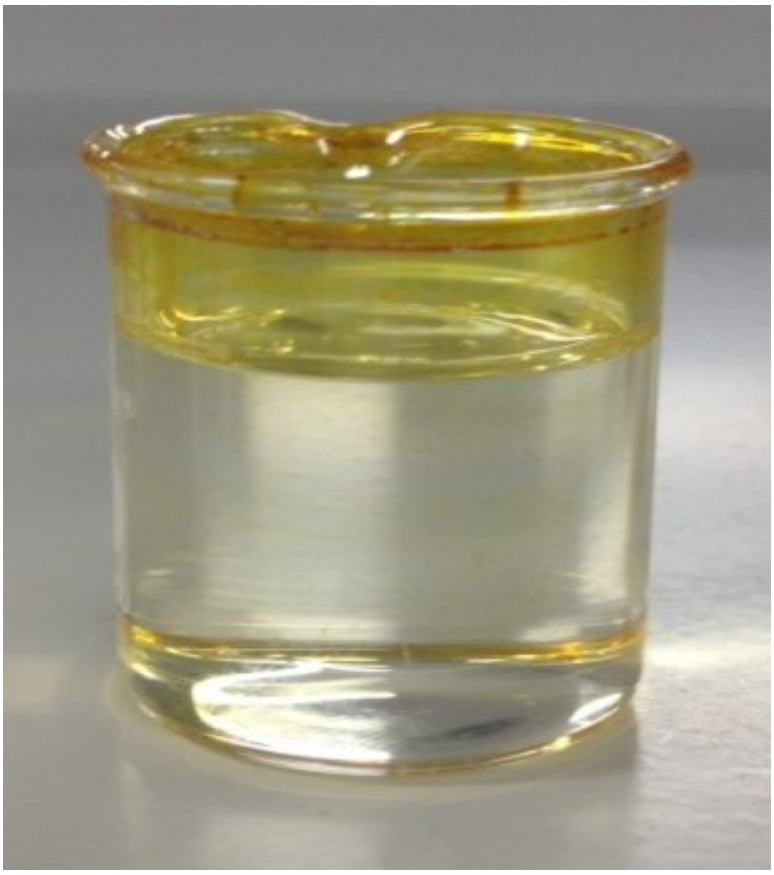

Figure 2.3: Coating solution of vanadium oxide

For the sub-zero temperature experiment the coating solution was kept at -10C for 40 min in order to deposit thicker films.

2.3 Dense films

The dense films (in the absence of a template material) were built up by depositing successively five layers of film leading to 160 nm thick films. The films were annealed at different temperatures after each layer.

2.4 Porous films

In order to create porosity in vanadium pentoxide xerogel prepared from a vanadium alkoxide, we have used polystyrene microspheres or a non-ionic polymer surfactant (Pluronic P-123) and heat-treated the dip-coated layers on ITO substrates at relatively high temperatures (400-500^{0}C).

2.4.1 Polystyrene microspheres (PS)

For the polystyrene microsphere templated films, the template was built up as follows:

The suspension of polystyrene microspheres (5.0% w/v) was sonicated for 15 min to assure the homogeneity of the suspension. 1-3 drops of the suspension were diluted in 10 ml of ethanol and the mixture was further sonicated for another 15 min to well disperse the microspheres in the solvent. The cleaned and dried substrates were placed vertically in small beakers containing the suspension of the microspheres in ethanol and kept at room temperature. Microspheres with a diameter of 0.63 and 1.0 μm were used in this work. The template is built up on ITO/glass substrates by thermal convection. After dip-coating, polystyrene microspheres were removed from the samples, either by annealing, or by extraction with tetrahydrofuran (THF).

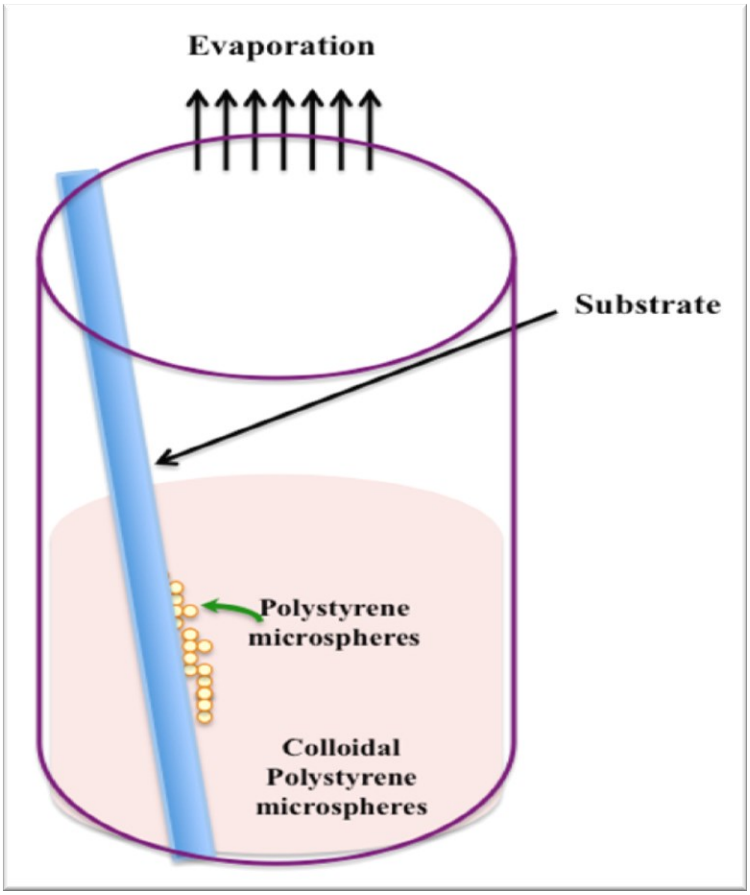

Figure 2.4: Thermal convection method for depositing the PS template

2.4.2 Triblock copolymer

The non-ionic surfactant, $EO_{20}/PO_{70}/EO_{20}$ (Pluronic P123) was dissolved in the coating solution (concentration of 2, 10, and 20%, respectively.) To remove the triblock copolymer at the end of the process, the samples were soaked in a mixture of water-ethanol (1:1) for 1 h, or they were heat- treated at high temperatures.

2.5 Deposition techniques

2.5.1 Dip coating

Coating by immersion is one of the simplest thin deposition methods, widely used for the controlled deposition of a variety of organic and inorganic compounds. The substrate is immersed vertically in the solution in small, 10mL beakers, at a constant speed and is totally

submerged to ensure an even coating on the substrate. Subsequently, the substrate is removed at a controlled rate, in order to obtain a uniform layer. The thickness of the film is controlled by the viscosity of the coating solution, the rate of withdrawing from the coating solution, the density and surface tension of the solution. The layer stays wet for several minutes until the solvent evaporates although this process can be accelerated by heat. The coating can be annealed by conventional heat, UV or IR techniques, and once a layer is, dry, another layer can be applied by immersion / annealing. By varying the number of cycles of soaking, the concentration and composition of the solution of coating, and the temperature of the coating solution (Room Temperature [RT] 27°C or Low Temperature [LT] -10°C), different thicknesses and film structures can be made. For example, dip coating is used to make thin films in manual assembly and the sol-gel method. Manual assembly can result in film of a thickness of one monolayer. The sol-gel method results in films that are perfectly controlled in terms of thickness, which can be controlled via the deposition speed and solution viscosity [53].

2.5.2 Steps of dip coating

There are three steps to the dip coating method (indicated in Figure 2.5, below):

- Submersion: the substrate is submerged in a coating material at a precise speed (45 mm/min)
- Submersion time: the substrate stays submerged and static to permit the coating material to fully encase the substrate (120 s).
- Removal: the substrate is removed at a constant speed (60 mm/min, because at this speed the uniformity of the film proved to be the best). It should be noted that a rapid removal results in a thinner coating.

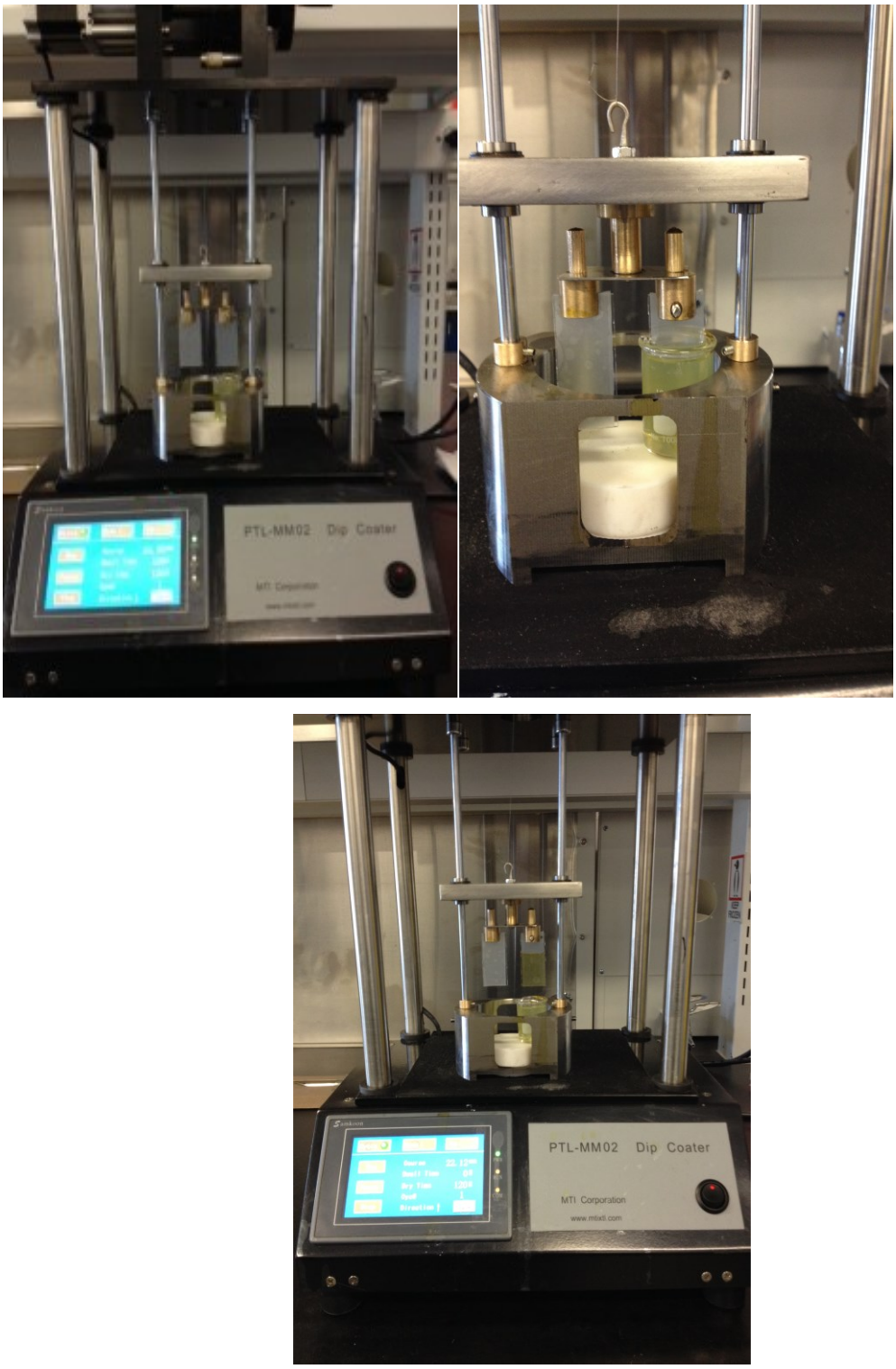

Figure 2.5: Steps corresponding to the dip-coating method

2.6 Electrochemical Cell

Figure (2.6) demonstrates the typical setup for the electrochemical characterization of the samples. The electrochemical cell has a diameter of 5cm and a height of 9cm (cylinder). The vanadium oxide film functions as the working electrode, with platinum functioning as the counter electrode, and a 0.1M lithium perchlorate solution as the ion-conducting electrolyte.

A three-electrode set up is generally used for the electrochemical measurements. The ITO substrate was put in contact with the lithium and then we deposited the working electrode onto the substrate, attaching the other side of the substrate to the electrochemical cell with screws. Silver/silver chloride (Ag/AgCl) is then submerged into the electrolyte to function as the reference electrode. This electrode is a AgCl coated Ag wire, with a Teflon cap and a porous Teflon tip from CH Instruments Inc. The potential is inserted between the working and reference electrode and the reaction (current or charge counter) is measured between the working and counter electrodes.

Using a non electrochromic material for the counter electrode and positioning it so that it does not disturb the incoming beam allows us to substitute the second transparent conductor with a non-conductive, transparent glass slide.

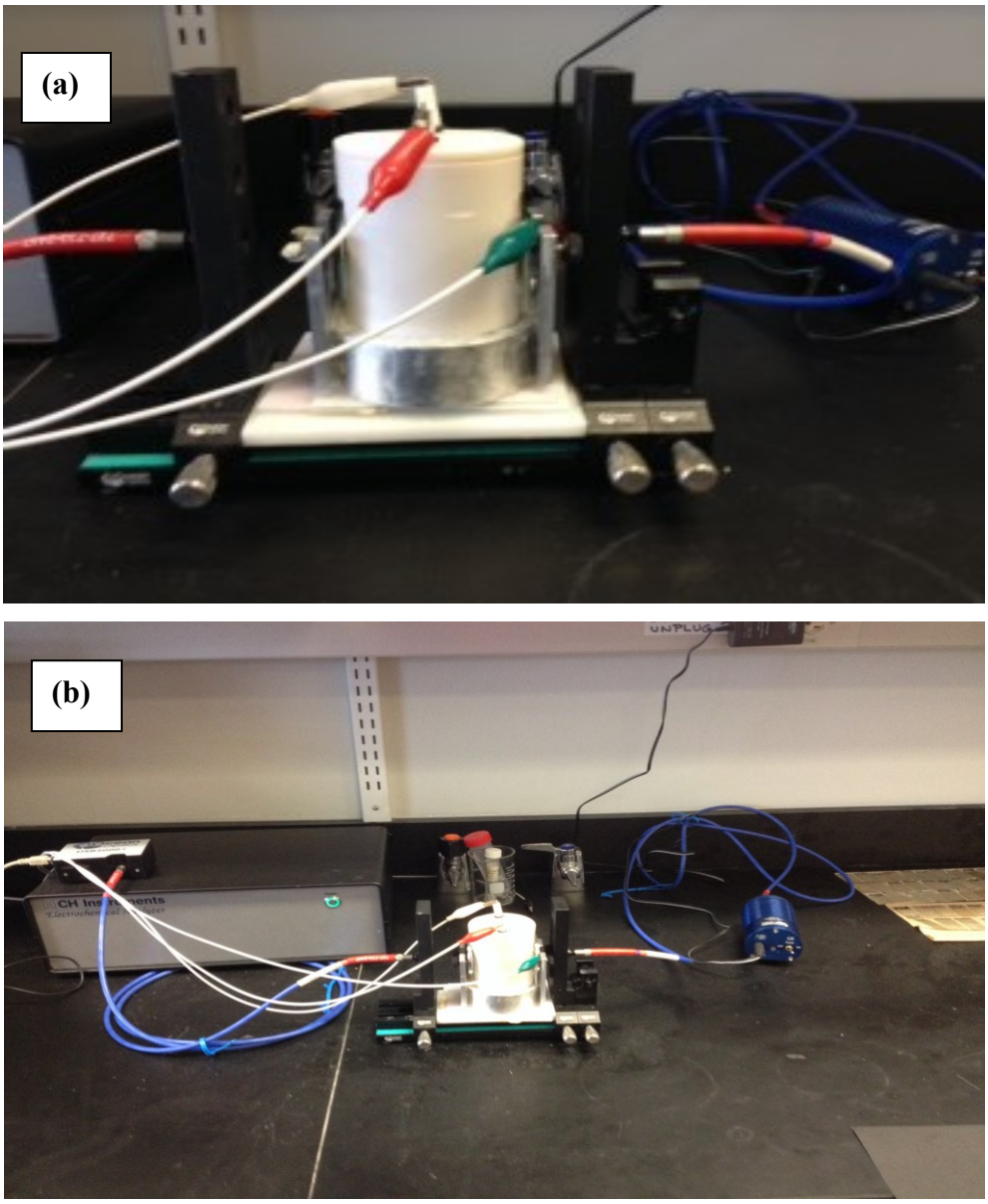

Figure 2.6: Device Setup

The connections from the electrodes are color coded and they go to the analyzer as shown in picture in Figure 2.6b

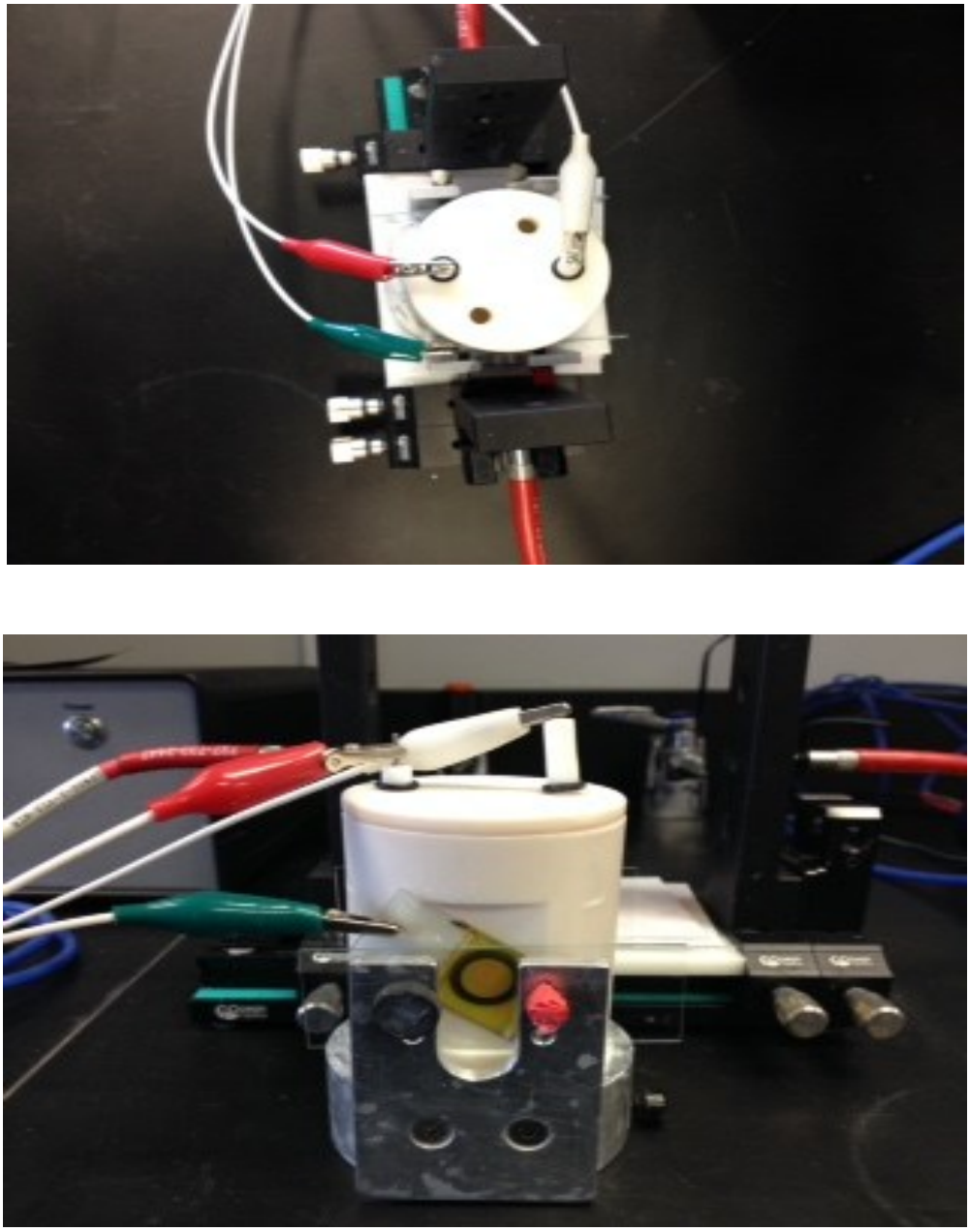

Figure 2.7: Top (upper) and cross-section view (bottom) of electrochemical cell device

2.7 Sample identification

Table 2.1a shows the parameters used for the fabrication of V_2O_5 films prepared either at room temperature or under the sub-zero condition (-10ºC), without using a template material. For each sample, the name, the number of layers (thickness), the temperature and duration of the heat-treatment are given. For the heat-treated samples, the concentration of the precursor solution and

the number of layers (the thickness) of films were kept constant. The samples with templates are described in Table 2.1b.

Table 2.1a Conditions used for the fabrication of V_2O_5 dense films

Sample	Number of layers	Annealing/drying temperature (^oC) and duration
A	1	27
B	5	27
C	10	27
D	5	200 for 60 min
E	5	300 for 60 min
F	5	400 for 60 min
G	5	450 for 60 min
H	5	500 for 60 min

Table 2.1b Conditions used for the fabrication of V_2O_5 porous films

Sample	Number of layers	Type of the template	Template removal method
I	5	PS 600 nm	Extraction
J	5	PS 600 nm	Annealing
K	5	PS 1000 nm	Extraction
L	5	Triblock copolymer, 2%	Extraction
M	5	Triblock copolymer, 10%	Extraction
N	5	Triblock copolymer, 20%	Extraction
O	5	Triblock copolymer, 20%	Annealing

Chapter 3

3 Characterization methods

3.1 Morphology and optical properties

Vanadium oxide films were characterized morphologically, by using SEM and AFM. The spectral properties of the films were determined by UV-Visible and Photoluminescence Spectroscopy. Raman spectroscopy was used to study the crystallinity of the film. The spectra were measured with a Renishaw Raman spectrometer (InVia) by using the excitation of a 514 nm Ar^+ laser. To determine the electrochomic properties of electrochromic materials, we used both electrochemical and optical methods, including cyclic/linear sweeping voltammetry, chronoamperometry, chronocoulometry and electrochemical impedance spectroscopy.

Scanning electron microscopy (SEM)

A Hitachi S-4700 Scanning Electron Microscope (SEM) was used to investigate the micro- and nano- structure of vanadium oxide films. Essentially, an electron beam is focused on the sample and the backscattered electrons are detected. The electrons emitted from the sample produce the SEM images. The number of electrons that reach the detector is dependent on the distance of the film from the surface and the topology and atomic weight of the films. Any variation in the thickness, smoothness or weight of the film will result in a variation in the contrast of the SEM images, which is why so much care is given to the creation of good surface conductivity. A layer of conductive material is coated onto nonconductive solid films to improve the image contrast through the prevention of the build-up of static electric fields on the surface. Coating is required for vanadium oxide films as they are usually semiconducting [54].

Photoluminescence spectroscopy (PL)

Because of the role of photons in this process, it is referred to as photoluminescence (PL). Once the photo-excitation phase is complete, a period of relaxation typically occurs where other photons are re-radiated. PL Spectroscopy is a popular method for analyzing the optoelectronic properties of semiconductors because it is efficient, non-destructive, contact free, and requires

very little sample manipulation. PL can provide detailed information on discrete electronic states, using both intrinsic and optical methods, while avoiding the errors and defects found when using practical semiconductor materials and extrinsic optical processes [55].

Raman spectroscopy

Raman measurements are used in this work to investigate the structural evolution, that is, the phase transformations during the heating process. The film crystallinity was studied using Raman spectroscopy. Raman spectroscopy is a method based on the inelastic scattering of monochromatic light. This scattering indicates that the application of monochromatic light to the sample alters the frequency of the photons. The~~se~~ photons are absorbed, then re-emitted by the sample. The Raman effect refers to the correlation between the shift, up or down, in the frequency of the reemitted photons and the original monochromatic frequency. This shift indicates the rotational, vibrational and other low frequency transitions in molecules. The narrow bands which are present in the spectrum at 300C and higher temperature belong to the crystalline face.

X-ray diffraction (XRD)

X-ray powder diffraction (XRD) is an instrumental method often used to study crystalline materials. To determine the phases in a given sample, an X-ray beam is focused onto these planes. Parts of this beam are then transmitted, some parts absorbed, other parts refracted and scattered, and some part diffracted. The diffracted portion of the beam allows us to measure the distances between the planes using Bragg's Law: $n\lambda=2d\ sin\theta$, where n is the order of the diffracted beam, λ is the wavelength of the incident X-ray beam, d is the distance between adjacent planes of atoms (the *d*-spacing), and θ is the angle of incidence of the X-ray beam. The *d*-spacing create a unique "fingerprint" of that samples' phases, and when interpreted properly, identifies the sample material. Amorphous material in the sample can be identified if a wide halo on the diffraction pattern is found.

3.2 Electrochromic properties

The electrochromic properties of the films were studied as a function of their thickness and annealing temperature. The films were dried in air after the deposition of each layer. The

voltammograms were obtained at a scan rate of 0.030 V.s-1 over a potential range of ±1 V. The electrochromic properties were evaluated through cyclic voltammetry and the optical modulation was measured simultaneously by UV-Visible spectroscopy. Chronocoulometry was used for measuring the intercalated charge. A three-electrode cell was used, where the V_2O_5 film on the ITO/glass substrate is the working electrode, Ag/AgCl the reference electrode, and Pt, the counter electrode. The electrolyte used in the experiment was a solution of $LiClO_4$ in propylene carbonate (1M). The electrochemistry of the surface depends on the species, the solution and the electrodes immersed in the solution. An electrode reaction involves the transfer of electrons between the two electrodes immersed in a solution where the transfer of electrons causes the transformation of a material between the forms of reduced and oxydated. In an electrochromic material, the working electrode's electrochemical reaction gives rise to a change in the color or transparency. The electrochemical properties of the oxide layers of vanadium oxide were determined using two techniques: cyclic voltammetry and chronoamperometry. Cyclic voltammetry applies voltages that vary linearly between two optimum states. In one, the oxide films have been reduced and transformed into a compound having a blue color, and in the other, they were oxidized to its original transparent state. The current flowing through the sample between the electrochromic material (a working electrode) and the counter electrode is measured and plotted against the voltage. In chronoamperometry, the potential, doesn't use linear time dependence, but rather is stepped up between two voltages for a set time, and then stepped back to its initial value. The current flowing through this sample is measured and plotted versus time. All electrochemical measurements were made with CH Instruments Inc. 604 D working electrochemical analyzer-station.

Cyclic voltammetry (CV)

The most common characteristic of voltammetric methods is the application of a potential to an electrode and following the current passing through the electrode, when determining the type of dissolved organic and inorganic substance. Various voltammetries include normal pulse voltammetry (NPV), cyclic voltammetry (CV), and square-wave voltammetry (SWV), all depending on the pulse method applied. CV potential is scanned linearly from the beginning voltage toward a higher (lower) voltage value in positive (negative) polarization with a certain scan rate, and scanned back to the initial value. CV is consists of two segments, controlled by

mass transport, the transport of electrons and a mixture of both. The first often comes from the movement of an ion in the presence of an electric field, either on account of a potential gradient, known as migration, or on account of a concentration gradient, known as diffusion, or both migration and diffusion may take place inside the films. However, the electron moves negative charges to the surface (the reduction reaction). The electron flow increases over time, until the surface concentration is neutralized. Subsequently, it begins to decrease (cathodic peak). At this stage, the process becomes broader. Similarly, an oxidation (anodic) peak also appears if the redox couple is reversible [56].

Impedance spectroscopy (EIS)

Electrochemical impedance spectroscopy (EIS) has been successfully used to understand the interfacial behavior in electrochemical systems. Various processes such as ohmic conduction, charge transfer, interfacial charging, mass transfer etc., can be separated, allowing a better understanding of the electrochemistry of the intercalation process.

Impedance, the strength of opposition to power in a circuit, is measured in the same units as the resistance. Unlike impedance resistance, resistance obeys Ohm's law, and can be monitored in DC circuits, where resistance is, for all intents and purposes, the impedance with zero phase angles on the non-alternating current.

Optical measurements

The insertion and removal of ions and load balancing electrons creates changes to the optical appearance of electrochromic films. The rate of the transfer of ions and electrons is reflected in the optical and electrochemical properties of the films. A tungsten halogen light source (Ocean Optics HL-2000), projects a light beam passing through the electrochemical cell to achieve this objective. A fiber-optic Spectrometer (Ocean Optics USB2000+) obtains the light from the opposite side of the electrochemical cell through the optical fiber so that it can be monitored. The resulting transmittance would then be:

$\%T_\lambda = (I_0/I_i) \times \%100$

Where: I_0 and I_i are the intensity of transmitted and incident light at wavelength λ, respectively.

In our study, the transmittance has been measured between 600 to 950 nanometers, in two ways:

- Transmittance vs wavelength at a specific time: this monitors optical performance of the electrochromic device. General optical modulation of the device can also be determined or measured.
- Transmittance vs time at a specific wavelengths: this alternate method provides detailed information regarding coloring and bleaching processes and at the inflection point. If ΔT_λ has a high value, the optical modulation at the wavelength λ is expected to be high, as seen in figure 3.1 below:

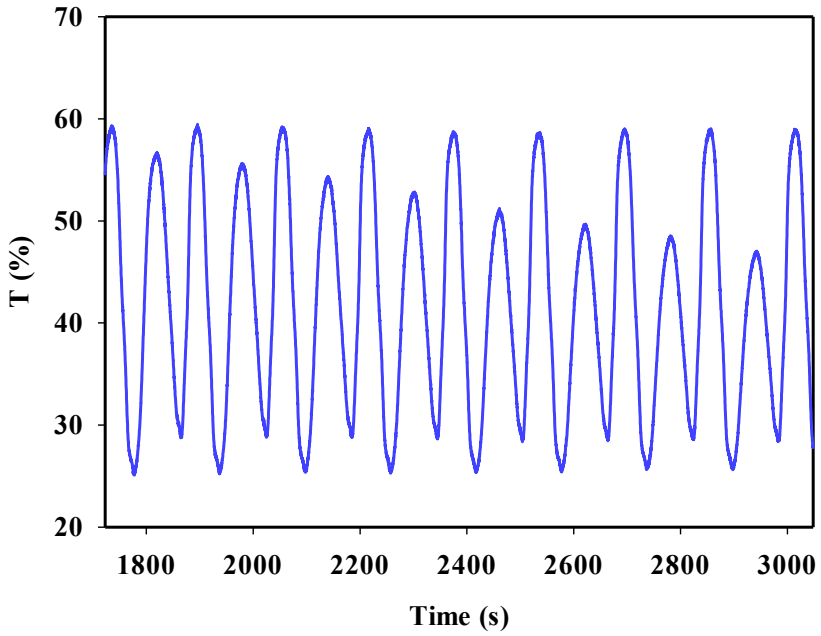

Figure 3.1: Optical modulation, the difference between the transparent or highest points, to the coloured state or lowest points in the figure

Key parameters for EC films

1. **Colouration efficiency (CE)**

CE is the ratio of the absorbance change per unit of inserted charge in the electrode area. The formula below is used to calculate this change in optical density.

$$CE = \frac{1}{Q/A} \ln\left(\frac{T_b}{T_c}\right) \quad (3)$$

where T_b and T_c are the transmittances of the bleached and colored states, respectively. The unit charge density (Q/A) is the charge consumed per unit electrode area and Q is the amount of charge intercalated, derived from chronocoulometry measurements.

2. **Diffusion coefficient (D)**

The rate of the diffusion of the lithium ions into the film is represented by the following formula. The film was cycled at different scan rates and the diffusion coefficients of Li^+ have been calculated using the Randles-Sevick equation as shown

$$i_p = 269000\, n^{3/2} A D^{1/2} C v^{1/2} \quad (4)$$

where:

i_p= current maximum (A)

n = number of electrons transferred in the redox event (usually 1)

A = electrode area in cm^2

D = diffusion coefficient in cm^2/s

C = concentration in mol/cm^3

ν = scan rate in V/s

The diffusion coefficient was calculated graphically, by calculating the slope (as shown in Figure 3.2), and introducing that number into the formula above.

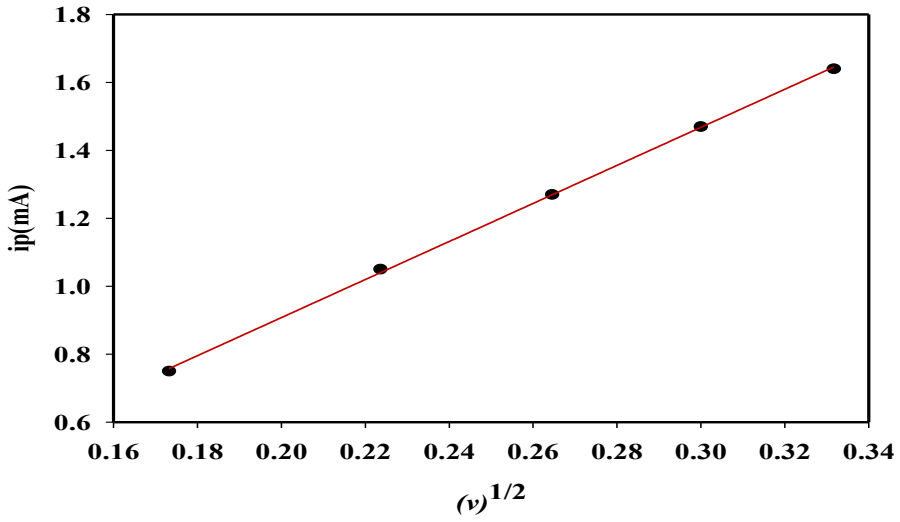

Figure 3.2: Maximum current (A) as a function of the square root of the scan rate (V/s)

Chapter 4

4. Results and discussions

This chapter will examine the results found from the various samples prepared; some films being among those identified in Chapter 2. While a large number of samples were analyzed, only a limited sampling is illustrated herein.

4.1 Vanadium pentoxide thin films dip-coated at room temperature

4.1.1 Vanadium oxide dense films prepared without a structure-directing molecule

Morphology and structural property

Sol-gel dip-coated films, without any structure-directing molecule, have been heated under the conditions specified in Table 1a in chapter (2).

Figure (4.1) shows the Atomic Force Microscopy (AFM) images corresponding to vanadium oxide films heat-treated at 500^{o}C (sample H in Table 1a).

In spite of the very thin layer (60-70 nm), the AFM image shown in Figure 4.2a reveals a few features that could not be seen previously in the Scanning Electron Microscopy (SEM) images of films dried at room temperature [57]. The image shows the presence of small spherical particles as well as of holes. The spherical particles appear better defined in the image 4.2b corresponding to the film heated at 300^{o}C [3].

Figure 4.3 shows that under the longer nanorods, particles and short rods can be seen. It seems that the transformation begins in the layers near to the substrate. This can be accounted for by the weak interaction of this layer with the substrate, the thermal energy forcing the separated layer to roll up. The nanorods are not oriented in a specific direction and their lengths are not uniform.

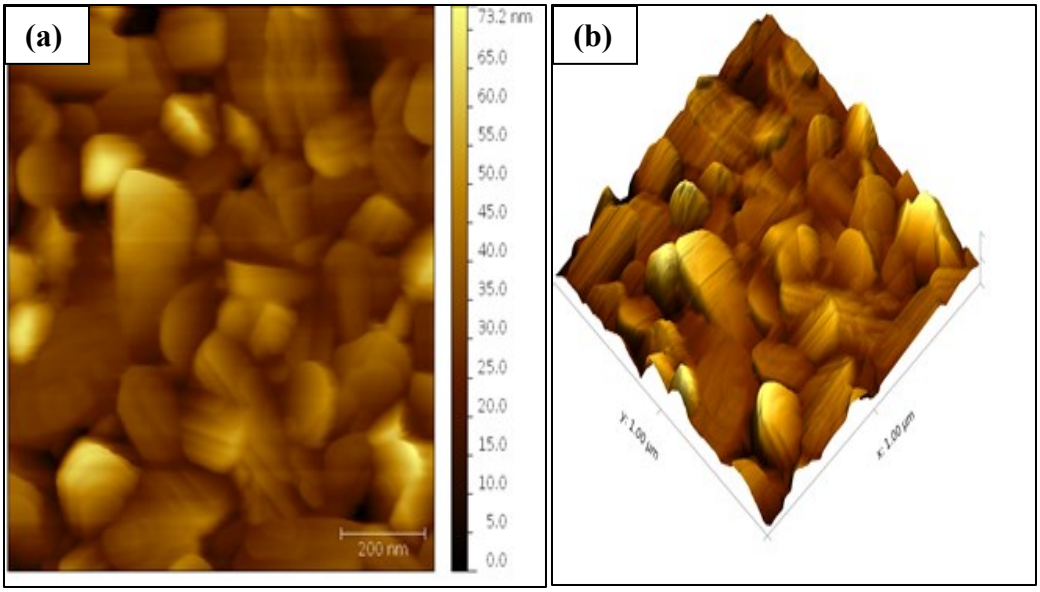

Figure 4.1: High resolution 2D and 3DAFM images of the V_2O_5 film heat-treated at 500^{o}C (sample H)

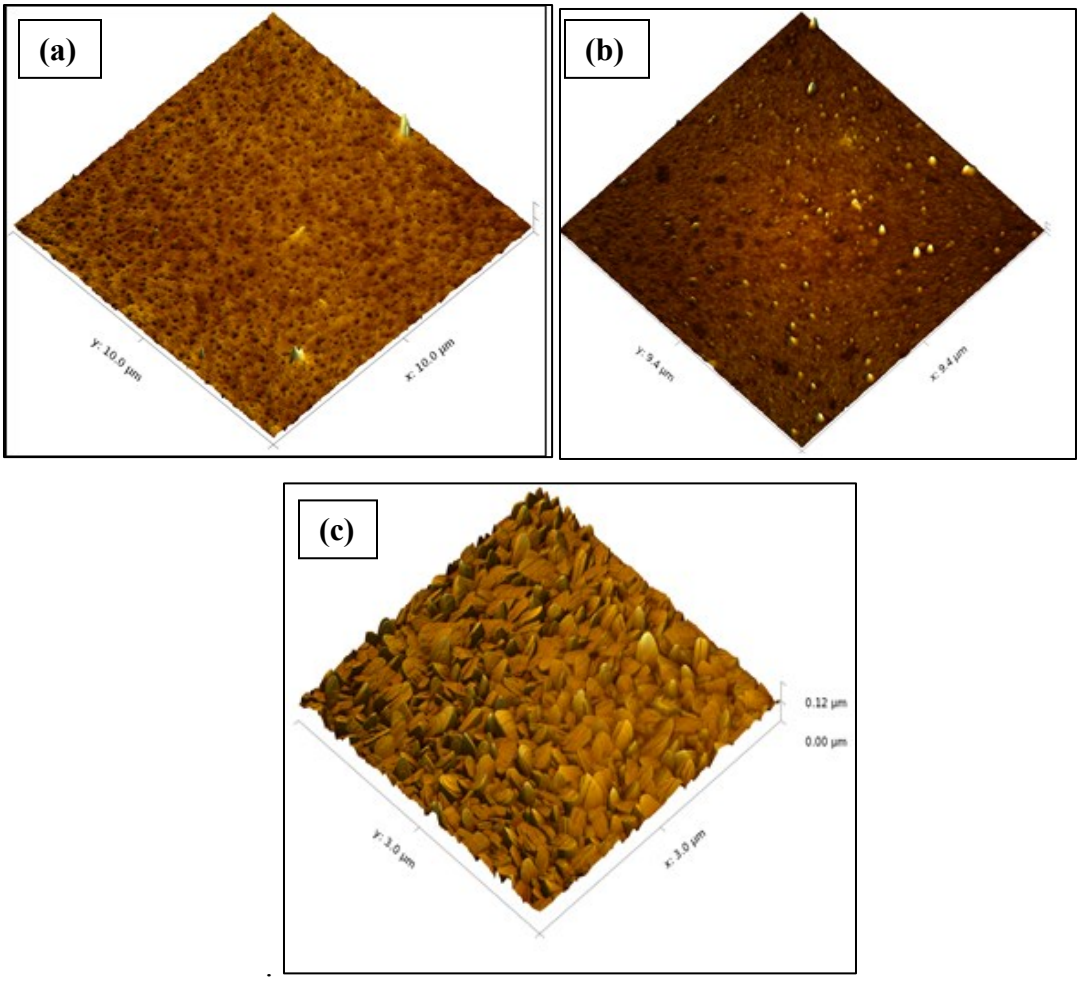

Figure 4.2: AFM images of the vanadium oxide films dried at room-temperature (a), heat-treated at 300^{o}C (b), and 500^{o}C (c)

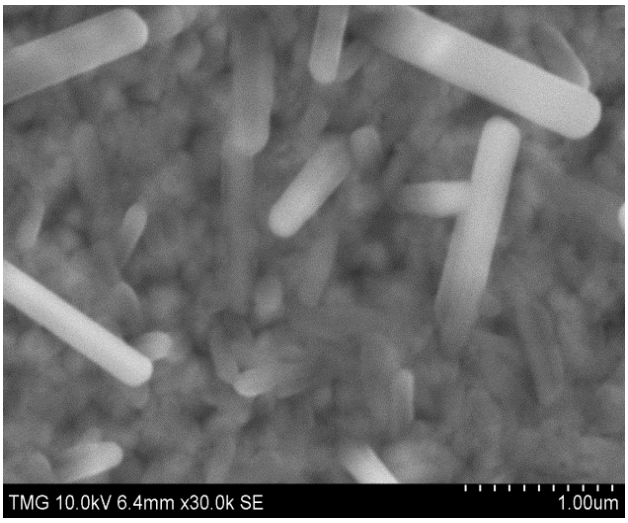

Figure 4.3: SEM image of the vanadium oxide film heat-treated at 500◦C (sample H)

Both AFM and SEM images (Figures 4.1, 4.3, 4.4 and 4.5) show that, in the case of a dense film, the temperature of 500^{o}C corresponds to a profound morphological transformation. After heating at 500^{o}C for a duration of 1h after each dip-coated layer, nanorods seem to grow out of the film. They can be seen more clearly in the SEM images shown in Figure 4.3 and Figure 4.4. The length of the nanorods is in the range of several microns and their widths are in the range of hundreds of nanometers. Figure 4.4 shows that the ends of the structures are closed and indeed, contrarily to some previous works, the prevalent structures found are nanorods and not nanotubes.

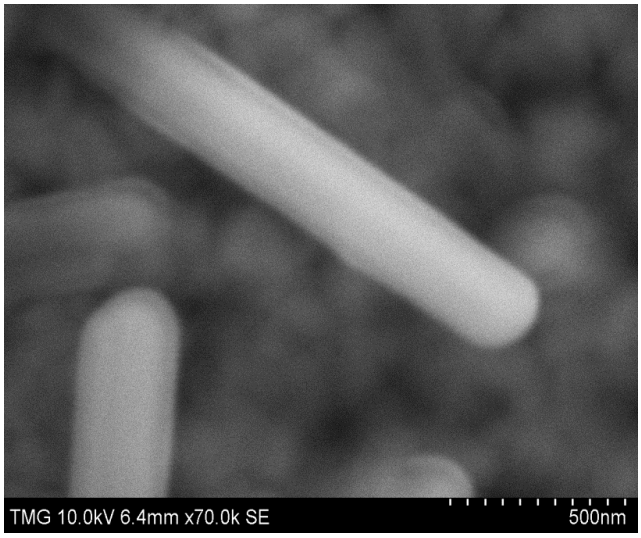

Figure 4.4: SEM image of one nanorod

Figures 4.5 shows the length of the nanorod is in the range of several microns and their widths are in the range of 20-50 nm or even wider.

Figure 4.5b shows that under the nanorod there is a smooth film from which the nanorods are growing out, breaking it. From this experiment it is not clear what happens to the superior layers but, nevertheless, it was worthwhile to investigate the optical and electrochromic properties of the samples with this particular morphology.

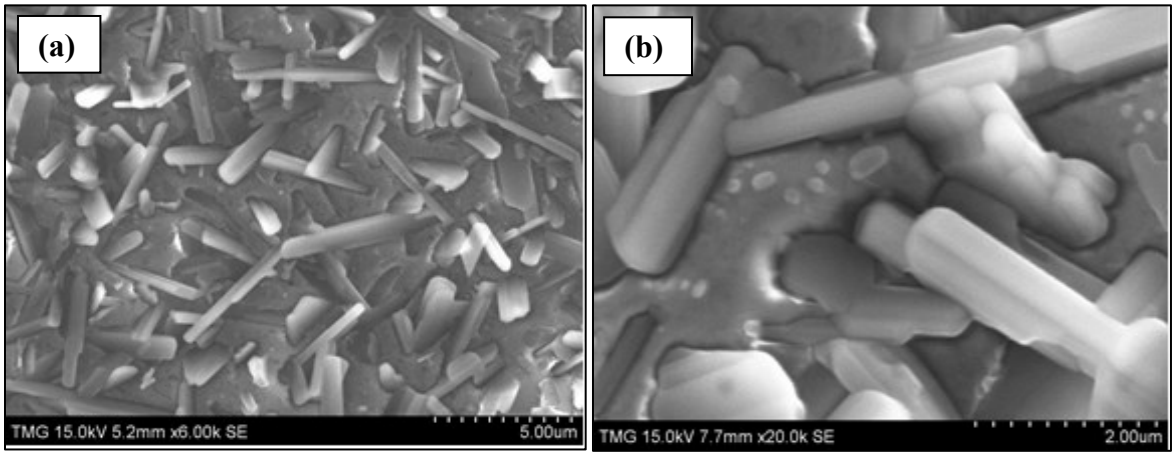

Figure 4.5: SEM images of the non-annealed dense film (sample H)

Figure 4.6 shows the XRD pattern of the dip-coated V_2O_5 film, annealed in air at 500^0C for one hour. The signal includes the contributions from the 66 nm thick V_2O_5 film and the ITO substrate. Reference patterns from the JCPDS database are indicated by the vertical lines. Based on a fit to the data (red line), the dimensions of the orthorhombic unit cell are a = 1.145 nm, b = 0.361 nm and c = 0.439 nm. Other authors have also reported orthorhombic structure for V_2O_5 films prepared by a sol-gel method [52, 37]. Based on the width of the diffraction peaks, the crystallite size is 23 nm. Annealing at 300^0C yielded a smaller crystallite size of 12 nm (data not shown) with unchanged unit cell dimensions. The nanorods crystalize in the orthorhombic system, but they are polycrystalline.

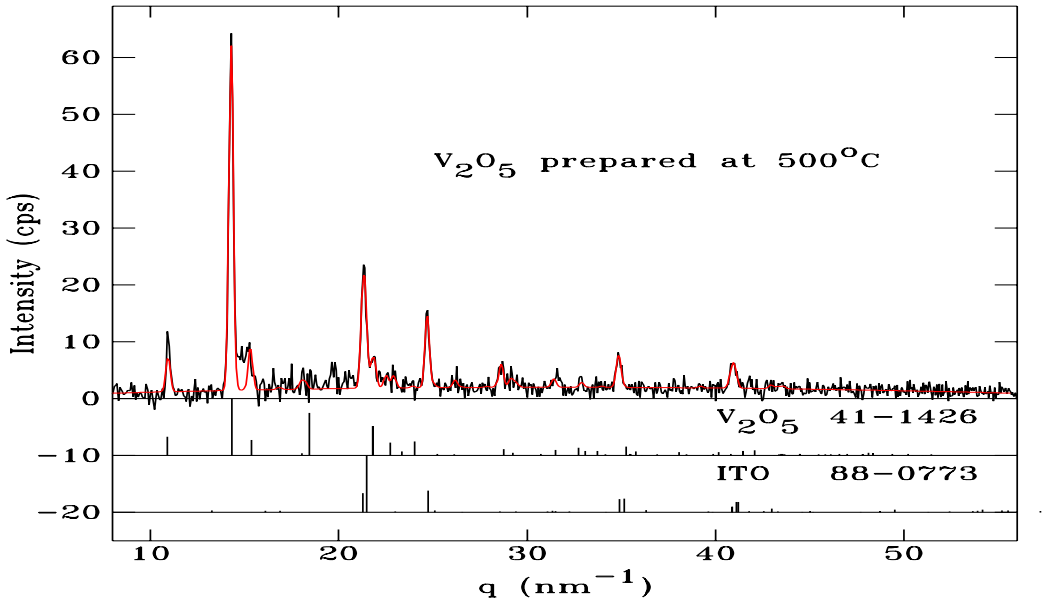

Figure 4.6: X-ray diffraction signal of an orthorhombic V_2O_5 film on an ITO covered glass substrate, annealed at 500^0C for one hour. The signal from the glass substrate has been subtracted. Below the JCPDS reference patterns are shown. The fit (red line) includes the contributions from V_2O_5 and ITO to the signal

Optical properties

The UV-Visible spectra of the vanadium pentoxide films annealed respectively at 300 and 500°C are given in Figure 4.7a together with the film dried at room temperature. Figure 4.7b shows the photoluminescence (PL) spectra.

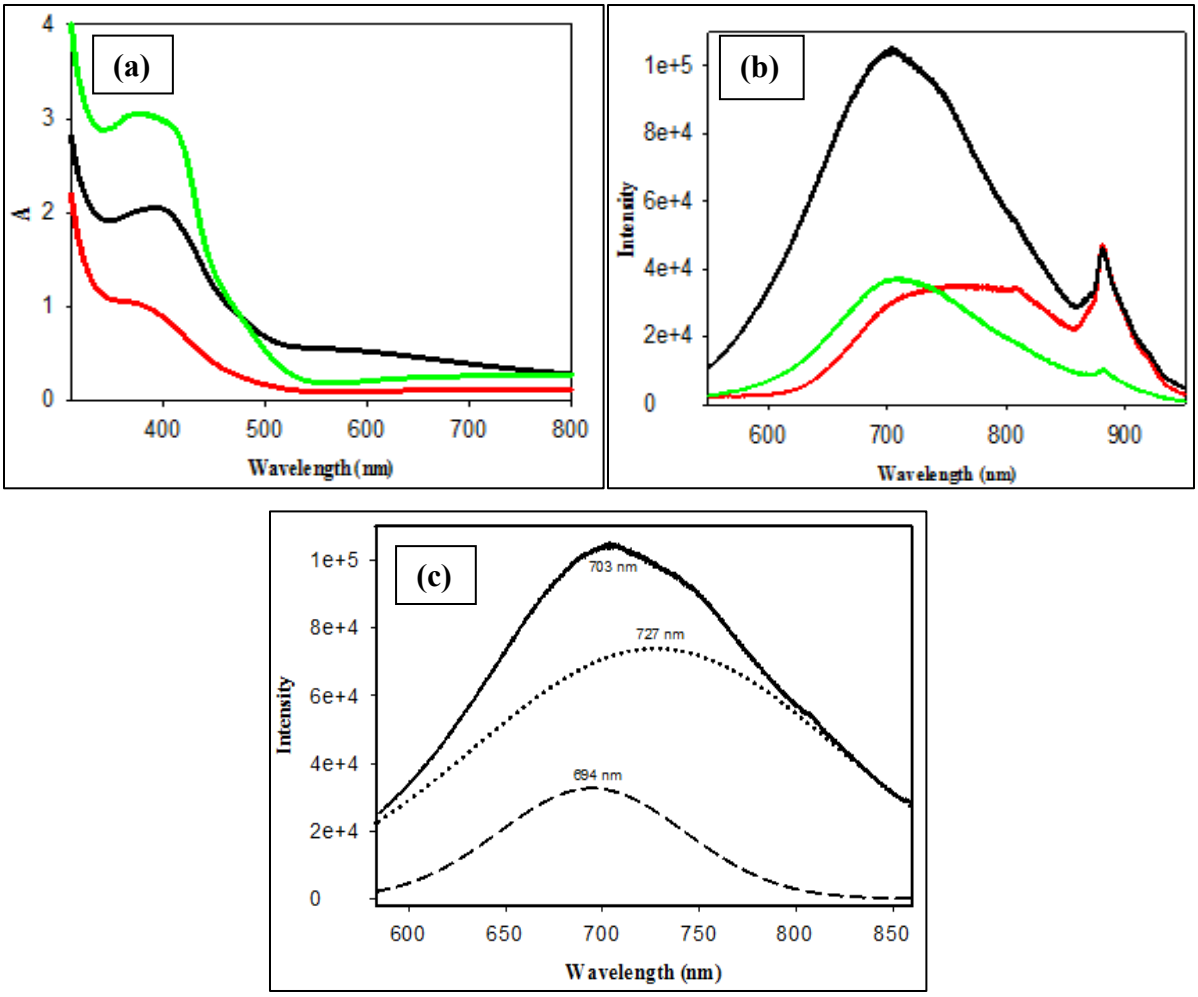

Figure 4.7: UV-Visible (a) and photoluminescence (b) spectra of samples B (red), E (green) and H (black), and (c) spectral deconvolution analysis of the PL spectrum for sample H

The spectrum shows that the band in the 350-400 nm region of the spectrum (Figure 4.7a) grows and becomes better defined as the temperature of the annealing increases. The band originates from the VO_4 species in tetrahedral coordination and it corresponds to an oxygen→vanadium charge transfer (CT) band, sensitive to the coordination of the central V^{5+}. When the coordination number is increased, the CT band shifts to higher wavelengths [57, 58]. Polycrystalline vanadium oxide can dissociate partially upon heating in the presence of air, resulting in V^{4+} defects. The PL spectrum (Figure 4.7b) shows a shift of the band, from 760 to 705 nm when the film is heated to 300^{o} C and the intensity of the emission at 700 nm is considerably higher than the case when the film is heat-treated at 500^{o}C in air. By a spectral

deconvolution analysis, two bands have been identified. Figure 4.7c shows the two fitted Gaussian bands (694 nm and 727 nm). It can be seen that the intensity of the PL band around 880 nm is slightly increasing with the annealing temperature. Taking into account the phase change observed at 500^{o}C, the high intensity of the visible light emission may be explained by oxygen vacancies or/and the V^{4+} defects that could appear during the formation of the nanorods [30, 58]. To our knowledge, there is no literature data regarding the sol-gel prepared nanorods.

Raman measurements are used in this work to investigate the structural evolution, i.e. the phase transformations during the heating process. Figure 4.8 shows the pattern of the Raman spectra for a non-heated sample (as-deposited) and for a sample subjected to thermal treatment at 300 and 500^{o}C, respectively. Non heat-treated samples show only broad bands corresponding to the amorphous nature of the sample. The characteristic bands of V_2O_5 appear in the spectrum of samples treated at 300^{o}C and become more prominent for the samples annealed at 500^{o}C. In the high-frequency region, the strong band at 1006 cm-^{1} corresponds to the V=O stretching vibration of the vanadyl unshared oxygen [59-60], the one at 710 cm^{-1} belongs to the stretching mode of the doubly coordinated oxygen (V_2 - O), and the band at 532 cm^{-1} corresponds to the stretching mode of the triply coordinated oxygen (V_3- O). The bending vibrations of the V=O bonds are located at 403 and 285 cm^{-1} and those of the V-O-V group, at 489 cm^{-1}. These bands correspond to the orthorhombic phase of V_2O_5 and their positions depend on the method of deposition and the history of the sample [60, 61]. Our results show that the characteristic bands of the orthorhombic α-V_2O_5 phase are seen after the thermal treatment at 300^{o}C and they coincide with the beginning of the formation of the nanorods [62]. Our Raman results on the crystallization are in agreement with XRD data on the sol-gel films [37-60].

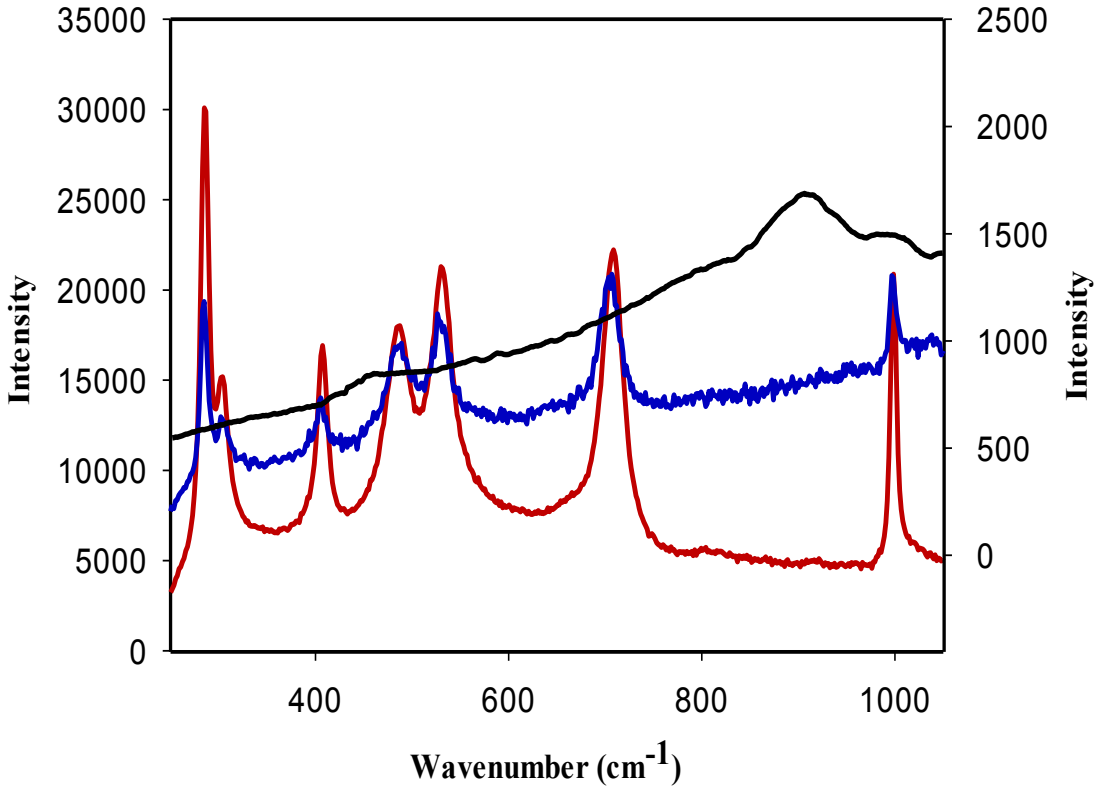

Figure 4.8: Raman spectra of vanadium pentoxide films without heat-treatment (black), annealed at 300◦C (blue) and 500◦C (red) (samples B, E and H). The y axis on the right side of the figure corresponds to the room temperature processed sample (B)

Electrochromic properties

The electrochromic properties of the films were studied as a function of their thickness and annealing temperature. Figure 4.9 shows the EC properties of the vanadium pentoxide films formed of 1, 5, and 10 layers, respectively.

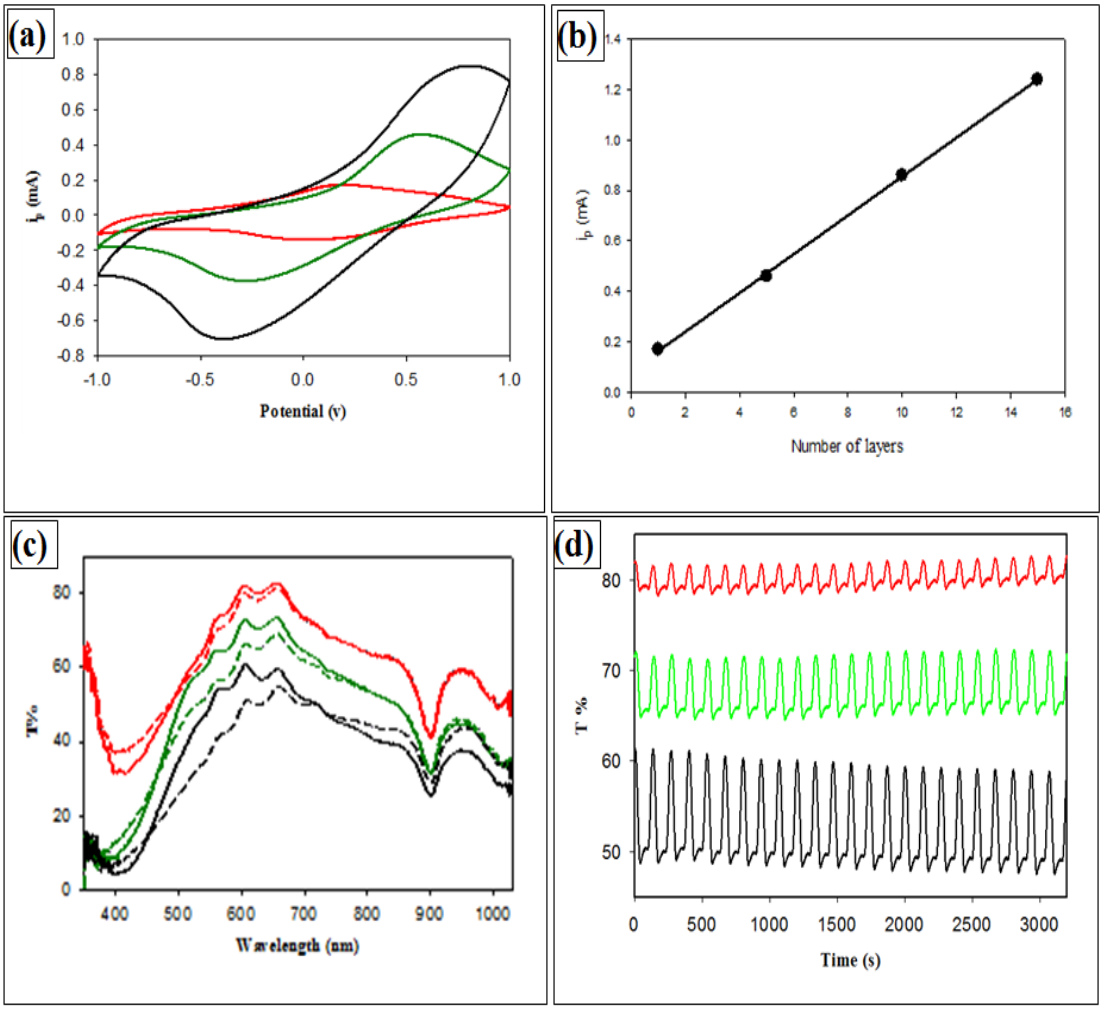

Figure 4.9: Electrochemical properties of vanadium pentoxide films as a function of the number of layers (1, 5, 10 layers, without heat-treatment) Cyclic voltammograms (a) Intensity of the current as a function of thickness (b), Transmission (c) and Optical modulation (----1 layer, ----5 layers, and ---- 10 layers) (d). The inset shows the color of the vanadium oxide film (yellow) and of the lithium bronze (green-blue)

The films were dried in air after the deposition of each layer. The voltammograms were obtained at a scan rate of 0.030 V.s-1 over a potential range of ±1 V. These particular films show only one couple of structureless redox peaks at around 0.70 V and – 0.4 V, ascribed to the V5+/V4+ pair. Figure 4.9b shows the linear increase of the current (i_p) with the number of layers and Figure 4.9c displays the optical modulation, i.e., the change in transmission when the films are colored by applying a voltage of -1 V and subsequently bleached under a voltage of 1 V. All samples

have shown an excellent reversibility. The measurements were made at 600 nm and the transmission of the three films is shown in Figure 4.9d. For the non-annealed films, the results show that the highest optical modulation is obtained in the case of the thickest film (10 layers). Table 4.1 shows the intercalated charge and the coloration efficiency (CE). The coloration efficiency, which represents the change in the optical density (OD) per unit of inserted charge (Q), was calculated by using formula (3) in Chapter 2.

The results (Figure 4.9) show that both the intercalated charge and the optical modulation increased slightly when the number of layers increased and resulted in a slightly increased coloration efficiency. The relatively low values of the intercalated charge may be attributed to the presence of the residual solvents and organic compounds at room temperature that obstruct the intercalation [63].

Table 4.1: Dependency of the coloration efficiency (CE) on the thickness of the film

Sample (no. of layers)	**Q (mC)**	**CE (cm^2/C)**
(A) 1	3.63	18
(B) 5	8.8	19
(C) 10	18	22

Because of the remarkable influence of the heat-treatment on the morphology and implicitly on the EC properties, a thorough investigation was undertaken to pinpoint the conditions to achieve the best CE and cycling stability of the films. Taking into account the profound morphological transformation shown by the AFM and SEM images, we have studied the EC properties of five layer films heat-treated respectively at 200, 300, 400, and 500^{o}C.

Figure 4.10a shows that the highest optical modulation was obtained by annealing the film at 300^{o}C when, as shown by the Raman data, the crystallization of the vanadium pentoxide started. However, at 400^{o}C, the CE is found remarkably high (Table 4.2) implying that the nanorods, emerging around this temperature, may actually promote the diffusion of Li ions into the film.

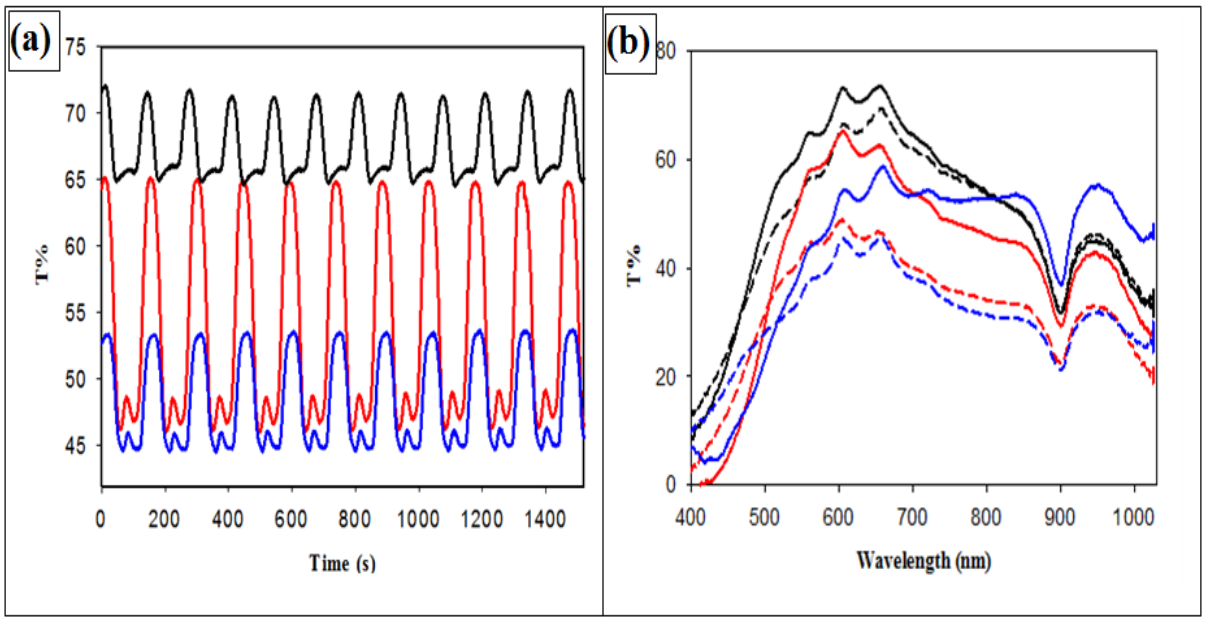

Figure 4.10: Optical modulation and transmission of 5 layer films without heat-treatment (black) and annealed at 300°C (red) and 500°C (blue). (Samples B, E and H). (Continuous lines represent the colored states and dotted lines the bleached states)

Figure 4.10a shows the optical modulation corresponding to a 5-layer film dried at room temperature and heat-treated at 300 and 500°C, respectively. For this film, the largest modulation is found when the film was annealed at 300°C as seen in Figure 4.10b as well.

Table 4.2 Dependency of the coloration efficiency (CE) on the annealing temperature.

Temperature of drying/annealing (°C)	**Q (mC)**	**ΔT (%) (600nm)**	**CE (cm^2/C) (600 nm)**	**ΔT (%) (843nm)**	**CE (cm^2/C) (843 nm)**
(B) RT	8.8	8	19	5	3
(D) 200	21.3	6	10	2	5
(E) 300	26.5	22	25	30	65
(F) 400	12.2	19	42	26	77
(G) 450	22.9	21	23	30	52
(H) 500	12.9	9	24	20	68

The results show that at 400, 450 and 500^{o}C, respectively, there is a sharp increase in the CE at 843 nm. Indeed both the intercalated charge and the optical modulation show considerably higher values when the film was heated at these temperatures.

4.1.2 Vanadium oxide thin film prepared with a structure-directing molecule

Effect of the heat-treatment on the morphology of vanadium pentoxide films prepared in the presence of a structure-directing molecule

Macroporous vanadium oxide films were prepared by dip-coating the solution on a polystyrene colloidal crystal template prepared by thermal convection as described in Chapter 2 Section 2.4.1. The results show that by removing the PS spheres through extraction with tetrahydrofuran (THF) a gentle, room-temperature method, the structure of the pores that replicated the microspheres was preserved. In addition to the large pores, a number of small pores can be seen at the contact area between the spheres as shown in Figure 4.11.a. A similar structure has been recently reported by Tong et al [63, 64].

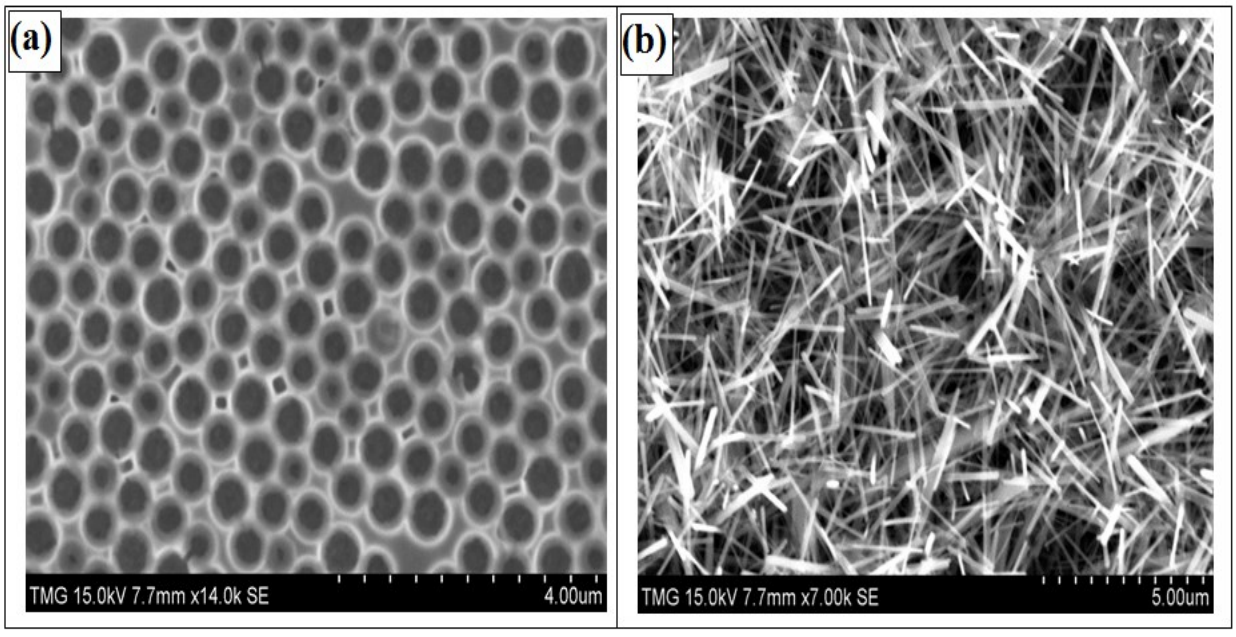

Figure 4.11: Effect of the method of removal of PS template on the morphology of the film (a) extraction of the template in THF under sonication (five layer film dried only at room temperature after each layer) and (b) annealing at 450◦C for 1 h (five layer films were annealed at 300◦C for 1 h after each layer)

However, when the sample was heated for a long time to remove PS (at 300^{o}C for 1 h after each layer and at 450^{o}C for 3 h at the end), instead of a layered structure, the same nanorod morphology emerged as in the case of the vanadium pentoxide without any structure-directing molecule (Figure 4.11.b). The SEM images in Figure 4.12 show that the same phenomenon happened in the case of another structure-directing molecule used in this work, the triblock copolymer- $EO_{20}/PO_{70}/EO_{20.}$

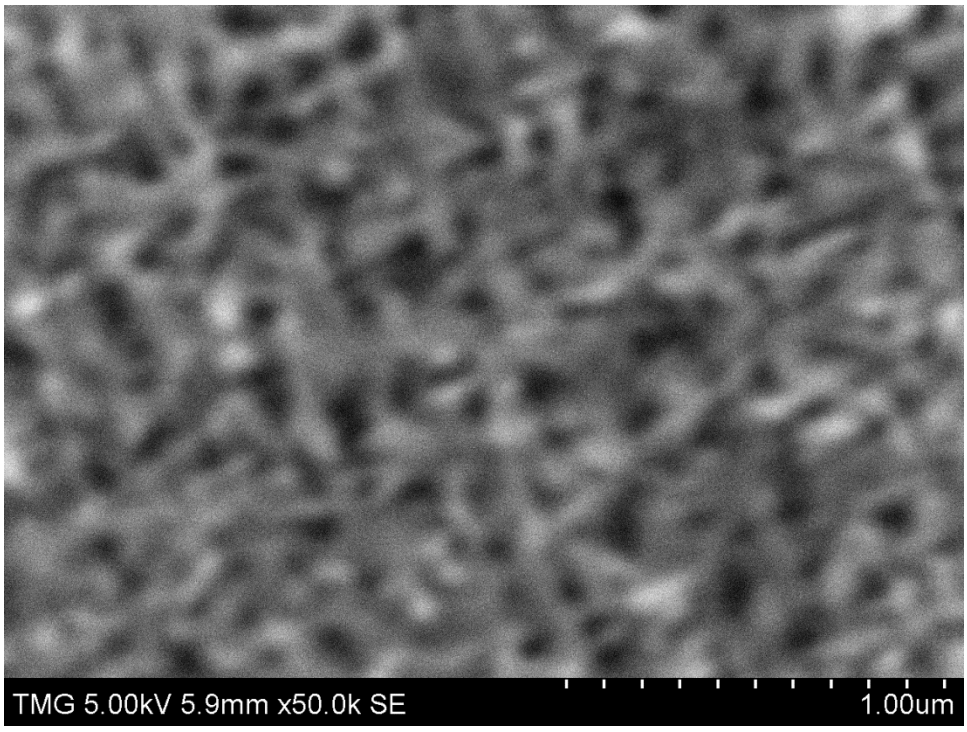

Figure 4.12: SEM images of V2O5 films prepared in the presence of 20% EO20/PO70/EO20 (Pluronic P123 - sample N)

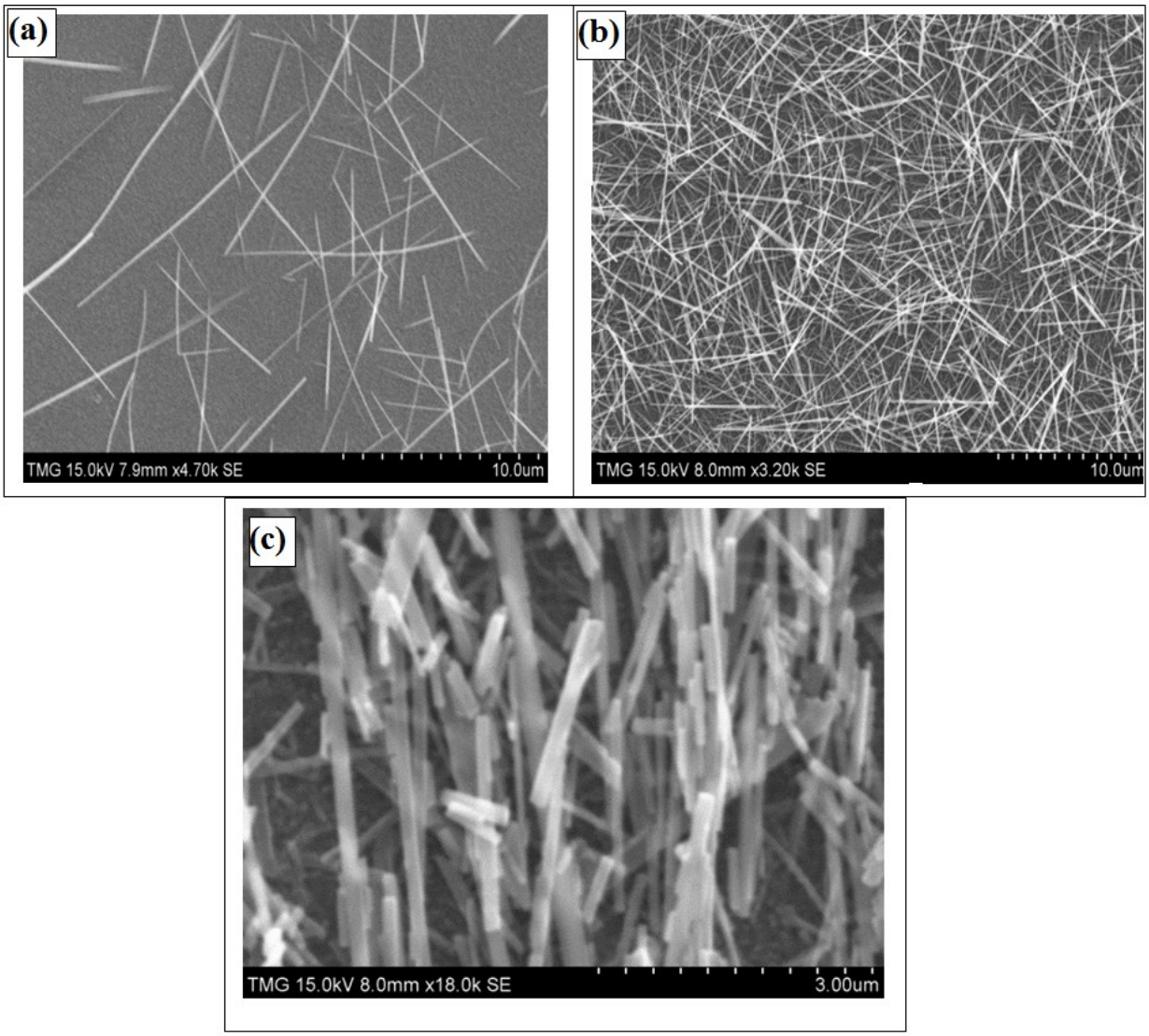

Figure 4.13: SEM images of V_2O_5 films prepared in the presence of 2% $EO_{20}/PO_{70}/EO_{20}$ (Pluronic P123) (a) 5-layer film, and (b) 10-layer film. Both films were dried in air between layers and annealed at 500^{o}C for 3 h to remove the template (c) a close view of the nanorods

Indeed, our results show that nanorods of V_2O_5 are formed in the process of removing the template, when the samples are annealed for a long time at temperatures higher than 400^{o}C.

As shown in Figure 4.13, the density of the nanorod films depends on the number of the coated layers, that is, on the amount of material. Further, we have investigated the electrochromic properties of porous films prepared under various conditions with structure-directing molecules.

Electrochromic properties of porous vanadium pentoxide films prepared with structure-directing molecules

The EC properties presented in this section correspond to porous layered structures as the processing of these films has been performed at room temperature. The inserted charge, optical modulation, the coloration efficiency and the diffusion coefficient for vanadium oxide films coated on PS colloidal crystals prepared with microspheres having two different sizes have been calculated.

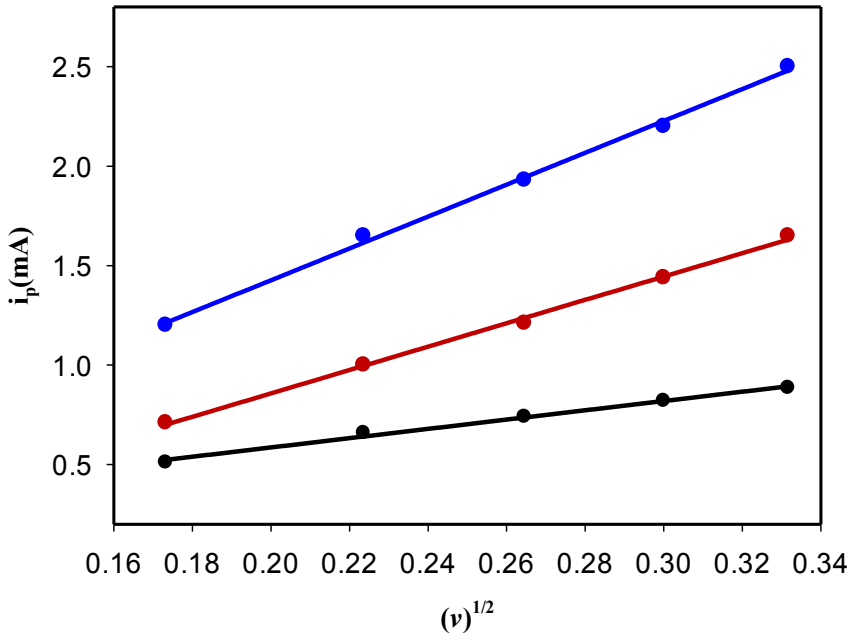

Figure 4.14: Dependency of the current on the scan rate for a dense film(black) and for both PS (600 nm) (red) and triblock copolymer-templated films (20%) (blue)

Figure 4.12 shows the SEM image of V_2O_5 films prepared in the presence of 20% EO20/PO70/EO20 (Pluronic P123 - sample N). The figure confirmed the high porosity of the film.

Figure 4.14 shows that intercalation of Li^+ into the vanadium oxide film is diffusion-controlled. The diffusion constant for the Li ion from the peak anodic current is calculated, using Randles-Servicik equation in Chapter 2.

The diffusion coefficient corresponding to the PS-templated films, together with the intercalated charge, the optical modulation and the calculated coloration efficiency are shown in Table 4.3.

Table 4.3: Effect of annealing temperature on the coloration efficiency of copolymer-templated films (nanorod structure)

Sample	**Q (mC)**	**ΔT (%) (600 nm)**	**CE (cm^2/C) (600 nm)**
Dense film	8.8	7	19
Templated (600 nm) film	14.7	30	35
Templated (600 nm) film (annealed at 450°C for 1h)	15.5	7	15
Templated (1000 nm) film	17.1	14	21

The values obtained for a dense film, prepared without any structure-directing molecule, are shown for comparison. The results confirm the higher coloration efficiencies of the porous films. In the films coated on polystyrene colloidal crystals, the lithium diffusion coefficients were found higher as compared to the dense film. The values are however lower than those reported by Tong et al. for porous films prepared with smaller spheres [67].

A triblock copolymer was introduced into the coating solution and removed from the film, either by soaking in a water-ethanol mixture or by annealing. The EC properties of the corresponding porous films were investigated and the diffusion coefficients were calculated.

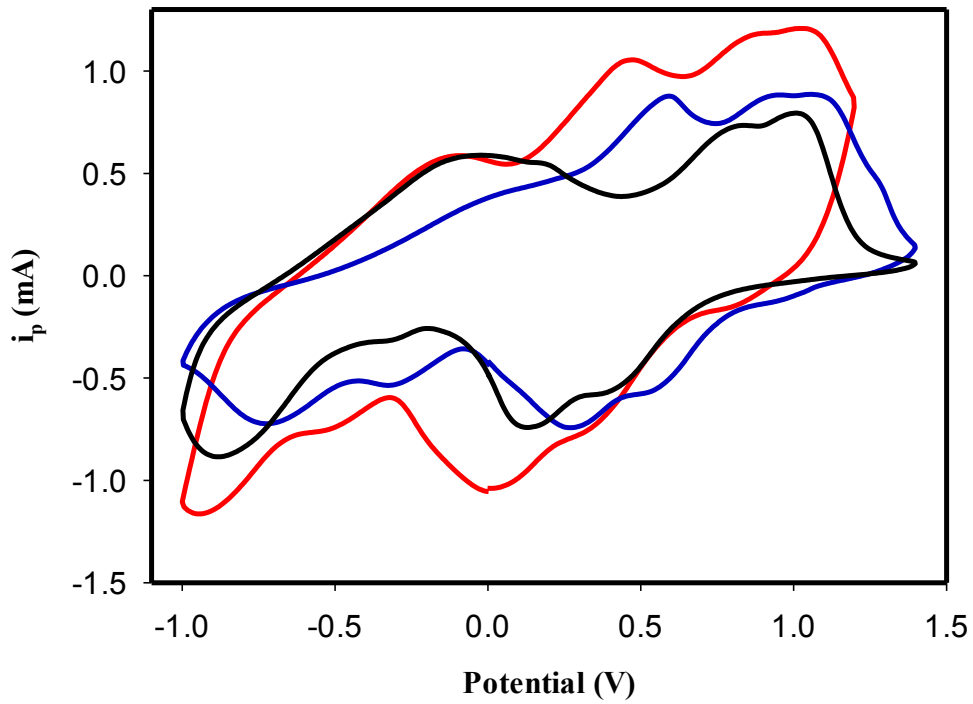

Figure 4.15: Effect of the amount of triblock copolymer template on the cyclic voltammogram (5 layer films, annealed at 300°C for 1 hr after each layer. The template was removed by soaking the film in a mixture of water and ethanol (1:1) for 1 h. (black – 2%, blue-10% and red-20%)

Figure 4.15 shows that over the -1.0-1.5 V potential range, the voltammogram shows at least three couples of redox peaks at potentials that depend on the concentration of the triblock copolymer. Compared to the two broad structureless peaks in the voltammogram of the dense film (Figure 4.9), the features seen in Figure 4.15 indicate a more effective and highly reversible Li intercalation and de-intercalation processes, respectively, in non-equivalent sites in V_2O_5. The diffusion coefficients in vanadium oxide prepared respectively with a PS and triblock copolymer templates were calculated from the slope of the corresponding graphs in Figure 4.14 and are given in Table 4.4.

These coefficients were found considerably higher than in the dense films (7.95×10^{-11}). The highest value corresponds to the sample with the highest concentration of triblock copolymer, having a larger porosity left behind after its removal [65]. The coloration efficiency (Table 4.4) of this film is the highest, demonstrating the role of film porosity.

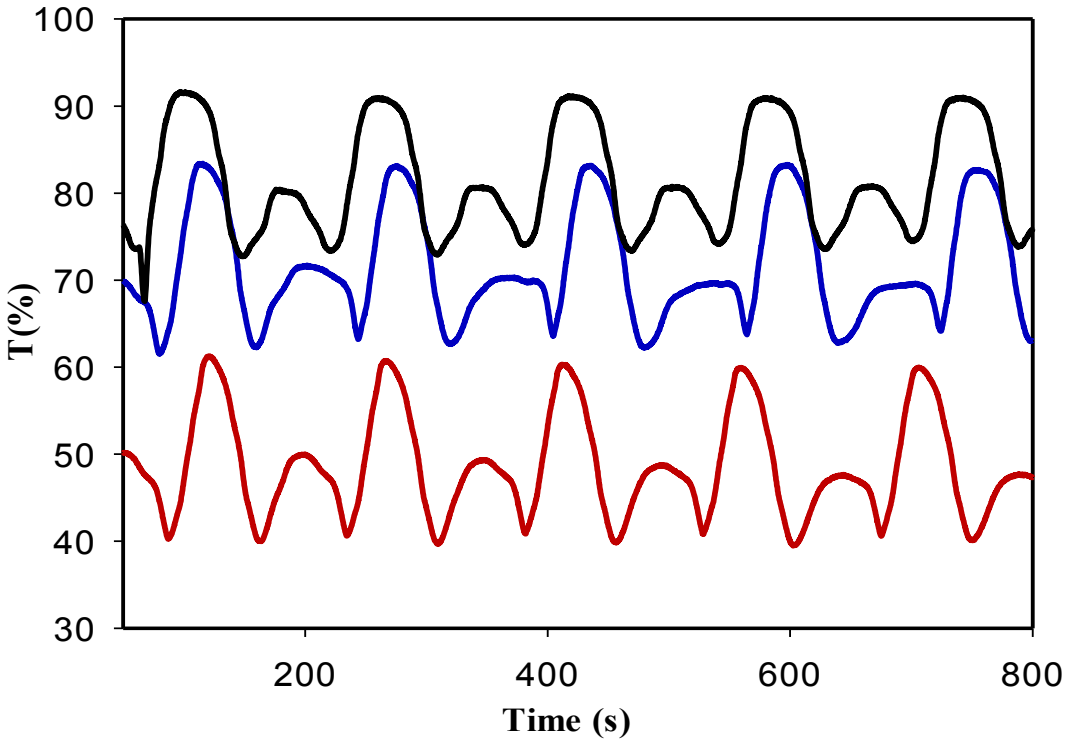

Figure 4.16: Optical modulations corresponding to the films with different amounts of triblock copolymer (black-2%, blue-10%, and red-20%)

Table 4.4: Effect of concentration of copolymer on the diffusion coefficient (layered structure)

Sample (concentration of copolymer)	**D (cm^2/s)**	**ΔT (%) (600 nm)**	**CE (cm^2/C) (600 nm)**
Dense film	7.95×10^{-11}	7	19
Templated (2%)	1.59×10^{-10}	18	25
Templated (10%)	2.00×10^{-10}	17	27
Templated (20%)	2.84×10^{-10}	20	57

As mentioned in the experimental part, the tri-block copolymer is a structure directing molecule creating a porosity in the film.

Cyclic voltammetry (CV)

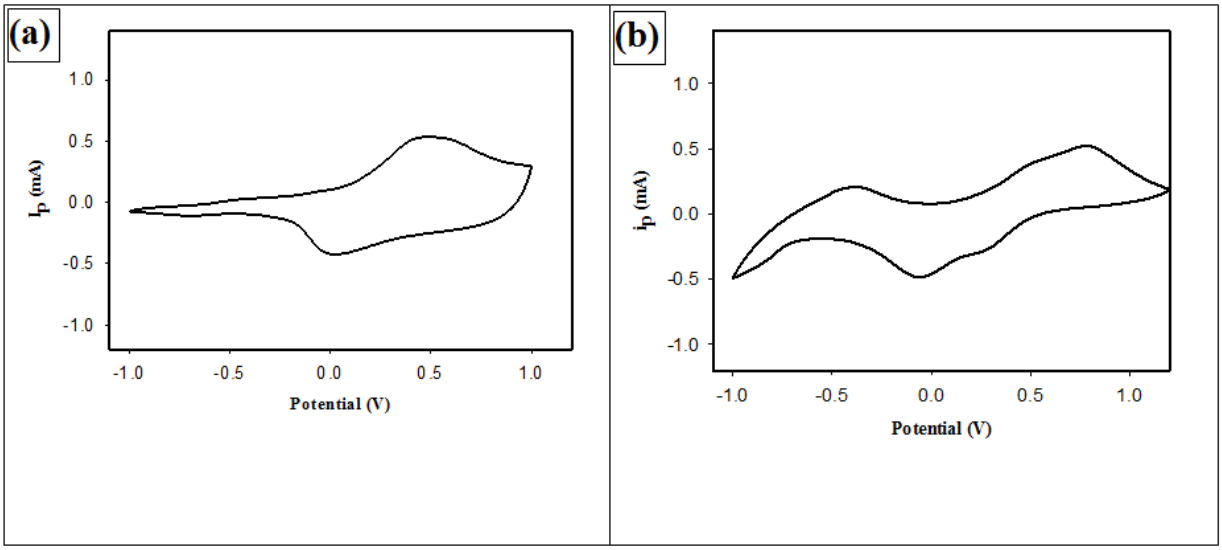

Figure 4.17: Cyclic voltammograms of a dense vanadium pentoxide film non-annealed (a) and annealed at 500^0C (b). The voltammograms correspond to the film stabilized electrochemically, after 25 cycles at a scan rate of 30 $mV.s^{-1}$

The voltammogram corresponding to the non-annealed film in figure (4.17a) shows a well-defined reduction/oxidation peak at 0.54 V and 0.055 V and weaker peaks at 0.775 and 0.261 V, respectively. The process shows an excellent reversibility. The voltammogram corresponding to the crystalline nanorod film has a more complex shape, with several reduction and oxidation peaks, corresponding to the progressive crystallographic phase transformation with increased lithium ion intercalation (0.79, 0.49, -0.42, -0.07 and 0.25 V).

Lithium insertion into vanadium oxide (during the cyclic voltammetry experiment) results in drastic changes in the crystal structure**.** Depending on the amount of inserted lithium, α- and ε-phases are formed for $x < 0.01$ and $0.35 < x < 0.7$ in $Li_xV_2O_5$, respectively. For a low content of lithium ($x < 1$), the phase transitions are reversible and, upon lithium de-intercalation, the original V_2O_5 structure can be recovered. However, for $x > 1$ the transformation from the δ phase into the γ-phase, becomes irreversible. This γ-phase can be reversibly cycled in the

stoichiometric range $0 < x < 2$ without changing the γ-type structure. If $x > 2$, this phase will be irreversibly transformed to the ω phase with a rock-salt type structure [20, 66].

In this kind of nanostructures, the electrolyte may be transported rapidly toward the intercalation sites. It has been shown, for example, that in thin nanoribbons the Li diffusion is three orders of magnitude faster than in bulk materials [1, 21].

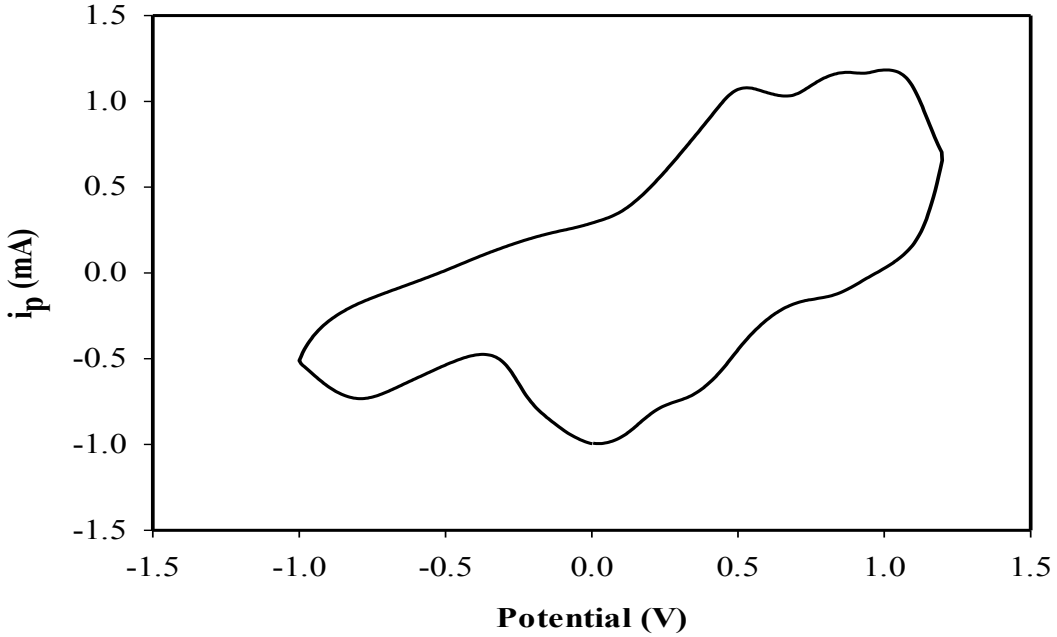

Figure 4.18: Cyclic voltammogram of a porous vanadium oxide film prepared with 20% triblock copolymer. The copolymer was removed from the film by extraction with a mixture of ethanol – DI water (1:1)

The distinct peaks observed in the voltammogram at 0.963, 0.37, 0.0106, 0.51, 0.836, and 1.03 V indicate a multi-step lithiation process.

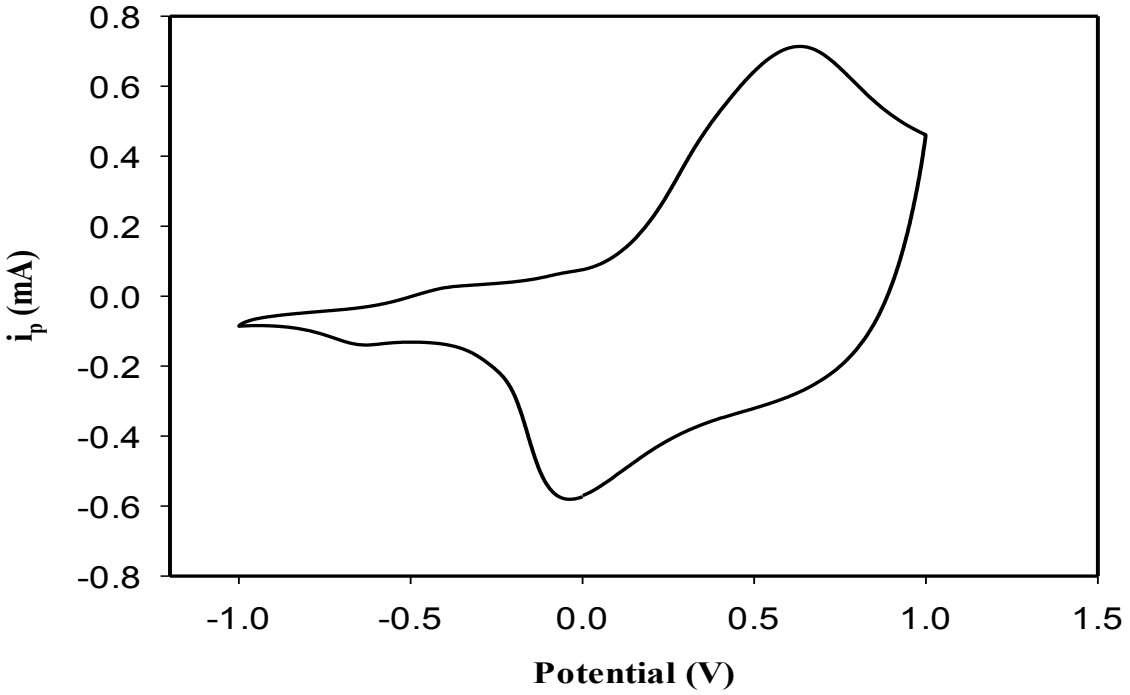

Figure 4.19: Cyclic voltammogram of a porous vanadium oxide film, prepared with a polystyrene microsphere template by using 600 nm microspheres. (The polystyrene microspheres were extracted from the film with tetrahydrofuran, at room temperature)

The removal of the microspheres leaves behind an extended multilayer network of uniform pores, having a size slightly smaller than the diameter of the original microspheres, due to the shrinkage of the network.

The voltammogram is similar to that corresponding to the dense film, with only one reduction/oxidation peak at 0.731 and – 0.004 V.

Electrical impedance spectroscopy (EIS)

The equivalent circuit that best fits the experimental data is Jin et al.'s model [67] and it is shown in Figure 4.20.

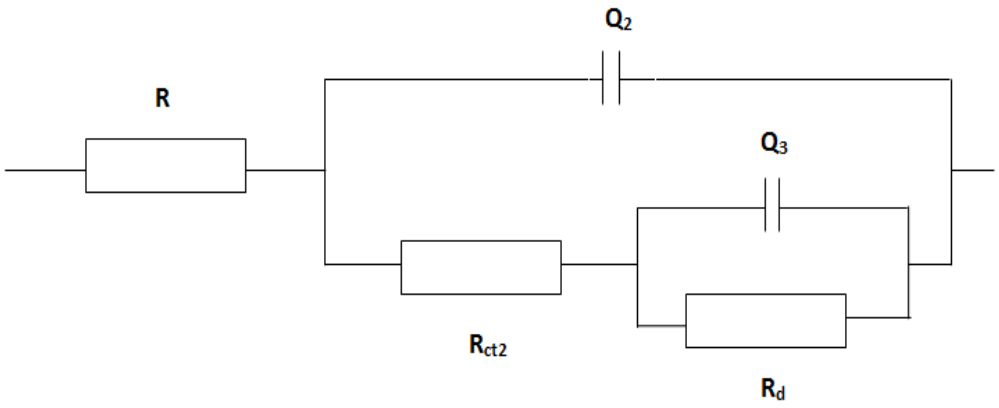

Figure 4.20: Equivalent circuit used to obtain the fitting parameters

In Figure 4.20, R_{ct2} is the sum of the ohmic resistance(s) of the solution and the vanadium pentoxide electrode, R_d is the ionic resistance due to the diffusion of lithium ions, R_{ct} is the charge transfer resistance due to the process occuring at the V_2O_5/solution interface. Q_2 and Q_3 are constant phase elements. CPEs model the behavior of an imperfect capacitor [67]. The electrochemical impedance spectra (Nyquist plots) corresponding to the four samples (see Table 2.1a and 2.1b) subjected to dc potentials of -0.5 and -1.0 V, respectively, are shown in Figure 4.21 – 4.24.

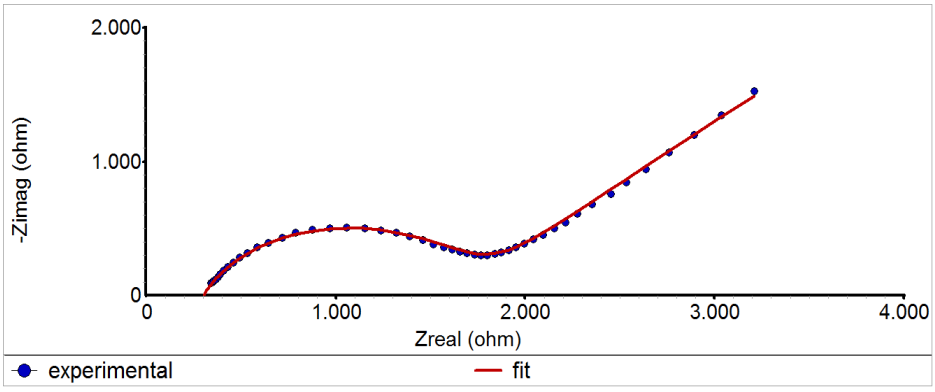

Figure 4.21a: Nyquist plot corresponding to the dense film (without a template), subjected to a dc potential of -0.5 V (sample B).

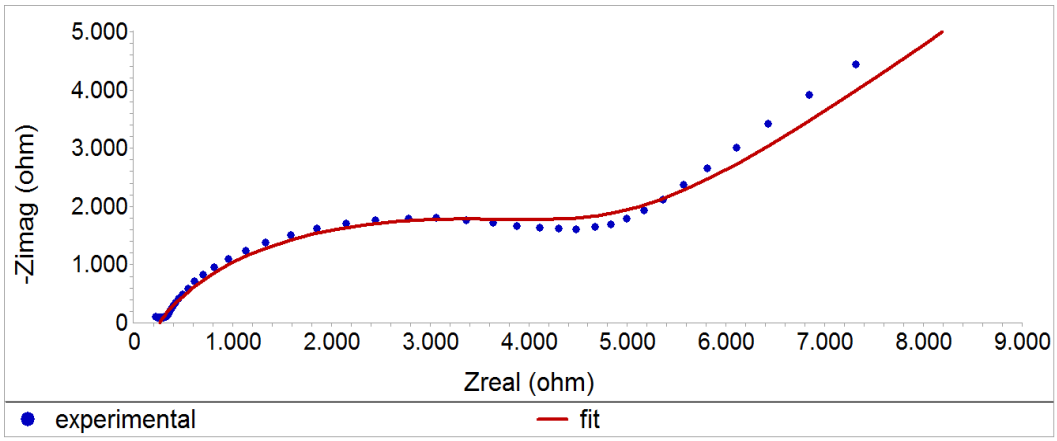

Figure 4.21b: Nyquist plot corresponding to the dense film (without a template), subjected to a dc potential of -1.0 V (sample B)

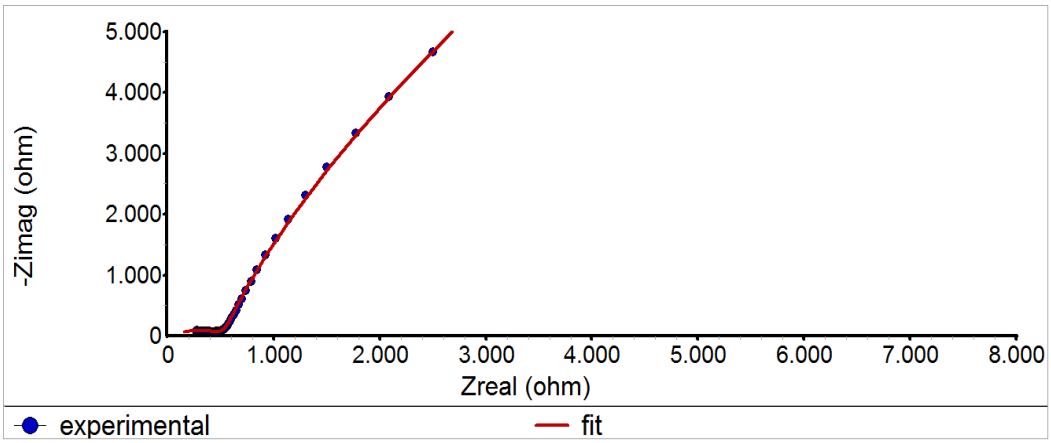

Figure 4.22a: Nyquist plot corresponding to the porous film, prepared with a PS template, subjected to a dc potential of -0.5 V (sample I)

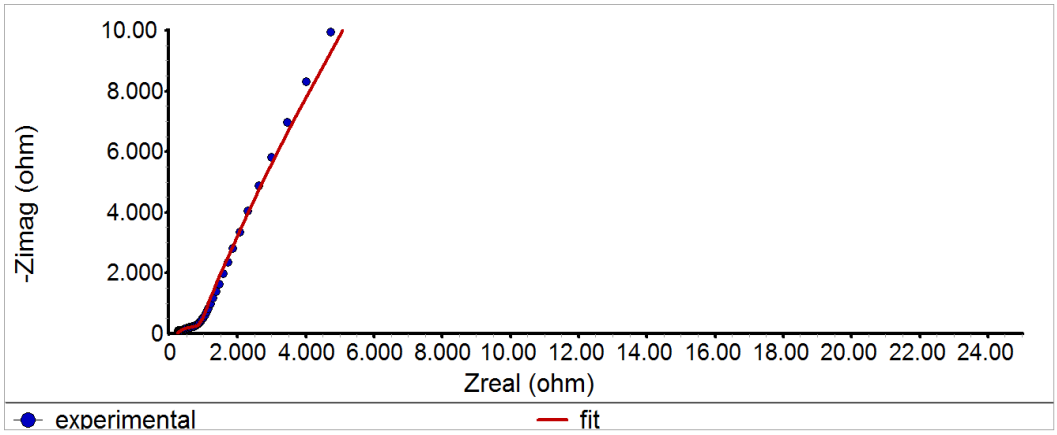

Figure 4.22b: Nyquist plot corresponding to the porous film prepared with a PS template, subjected to a dc potential of -1.0 V (sample I)

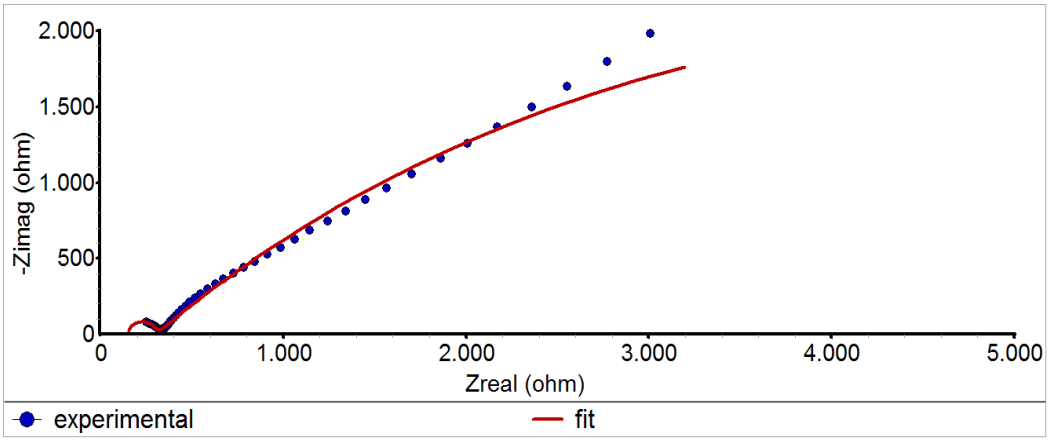

Figure 4.23a: Nyquist plot corresponding to the porous film prepared with a triblock copolymer template, subjected to a dc potential of -0.5 V (sample N)

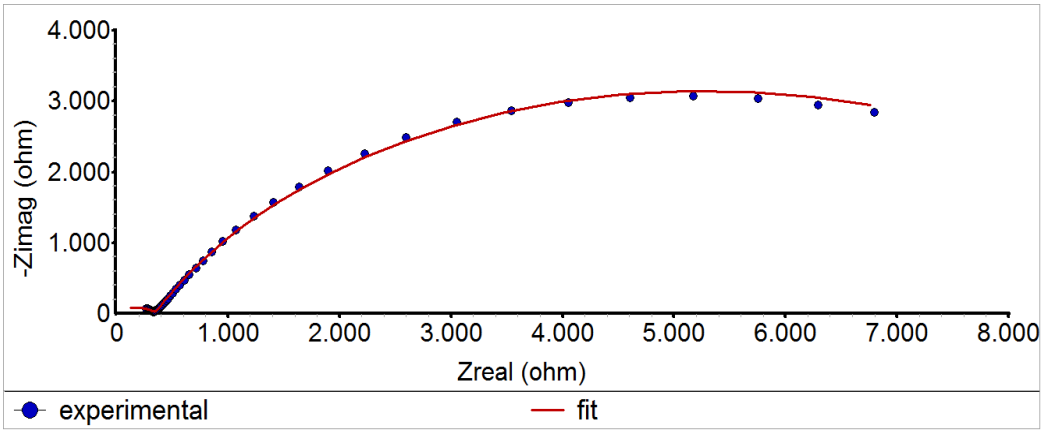

Figure 4.23b: Nyquist plot corresponding to the porous film prepared with a triblock copolymer template, subjected to a dc potential of -1.0 V (sample N)

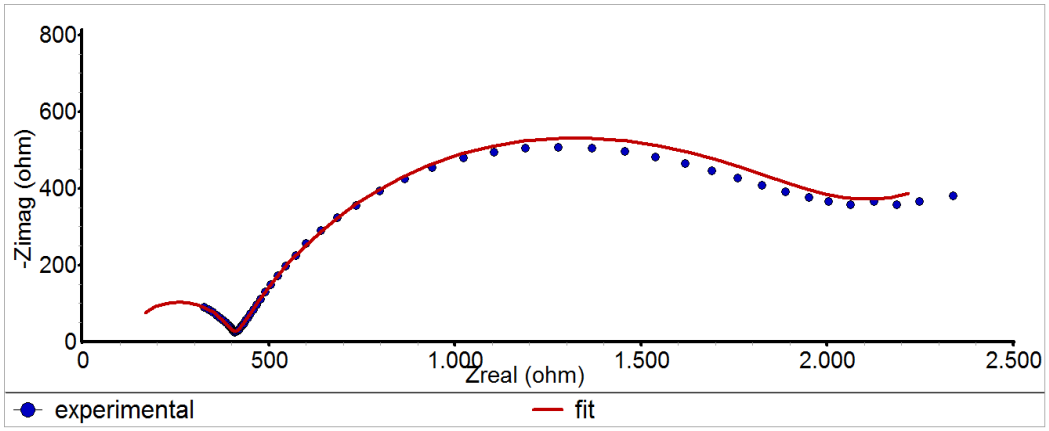

Figure 4.24a: Nyquist plot corresponding to the film prepared without a template and annealed at 500^0C (nanorod film), subjected to a dc potential of -0.5V (sample H)

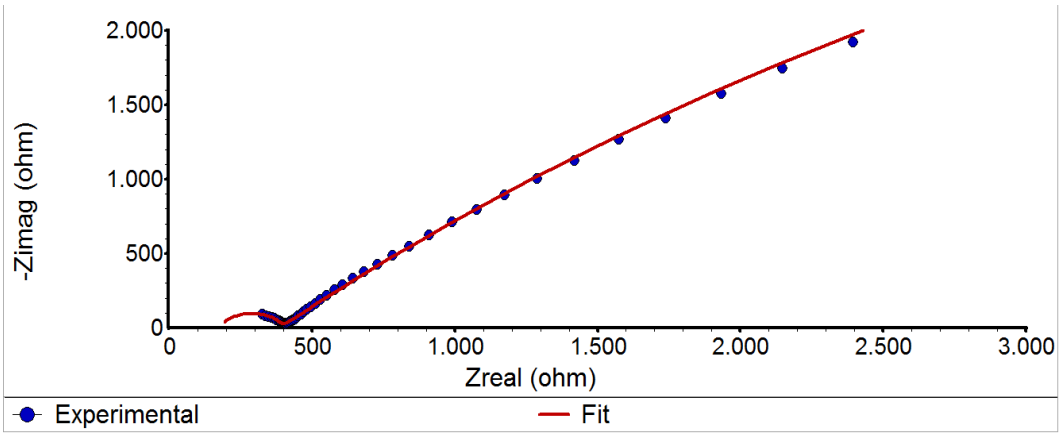

Figure 4.24b: Nyquist plot corresponding to the film prepared without a template and annealed at 500^0C (nanorod film), subjected to a dc potential of -1.0 V (sample H)

Generally, for all of the samples, in the high frequency range, the impedance spectra consist of a depressed arc and, in the low frequency range, a straight line with a phase angle of 45^0. The high frequency arc is usually assigned to the charge transfer at the electrolyte/electrode interface, while the inclined line in the low frequency range is due to the Constant Phase Element, associated with the semi-infinite diffusion process of lithium ions through the vanadium oxide film. The presence of the charge transfer semicircle in the high frequency range does not depend on the degree of lithium intercalation [67].

Our results show that, in some of the samples (for example the porous film prepared with polystyrene microspheres), the phase angle is higher than 45^0, indicating a faster diffusion of Li ions, compared with the other samples.

The high frequency arc is severely depressed in some of the graphs, for example in Figure 4.22 and in a slighter extent, in Figure 4.23, as a result of the porous character of the corresponding sample. The degree of depression of the high frequency arc is determined to be 0.7- 0.8, by using the parallel combination of a resistor and a constant phase element (CPE). In order to consider depressed semicircles, the commonly used capacitor is replaced with constant phase elements Q_i. The CPE had been the object of many discussions in the literature, and a discussion of its significance is beyond the scope of the present work. The CPE is calculated with the formula:

$$Z(Q_i) = 1/Y_i (j\omega)^{-n_i},$$

where ω is the angular frequency, and Y_i, j and n_i are constants.

The location of the Warburg impedance (the frequency range) appears to be shifted toward higher frequency when the degree of insertion of Li^+ is higher. This is in agreement with Vivier et al.'s observation for the case of lithium insertion in crystalline vanadium pentoxide thin films [67]. The shift of Z_W was accounted for by the evolution of the diffusion coefficient, D_{Li}, with the composition (x in $Li_xV_2O_5$).

The charge transfer resistance (R_{ct2}) is the most important parameter related to the V^{5+}/V^{4+} reduction process occurring at the electrolyte/vanadium oxide film. Table 4.5 shows the values found by curve fitting for the dense and porous samples as well as their dependency on the applied dc potential. The result show that, in general, the values of R_{ct2} are increasing with the applied potential but the changes appears to be more significant for the dense film (non-templated) and for that templated with polystyrene microspheres (1450 to 4600 Ω and 593 to 875 Ω, respectively). Only a slight dependency on potential was found for the samples templated with the tri-block copolymer and the non-templated, annealed to 500^0C (153 to 173 Ω and 185 to 206 Ω, respectively). Jin et al. [67] suggested that the decreased conductivity is due to an excess of V^{4+} sites over the V^{5+} sites, corresponding to a higher degree of lithium intercalation. At the same time, the electrostatic repulsion between the lithium atoms restricts their mobility.

The low values of R_{ct2} corresponding to the copolymer-templated and the 500^0C- annealed samples, found by the impedance measurements, show a good agreement with the high mobility of Li^+ found for these samples ($D = 3.3x10^{-10}$ and $D = 2.84x10^{-10}$ cm^2/s, respectively). The high values found for the coloration efficiency (see Table 4.4) confirm as well that the electrochromic properties are strongly correlated with the charge transfer resistance R_{ct2} determined from EIS measurements.

The parameters estimated through curve fitting are summarized in Table 4.5.

Table 4.5 Fitting parameters corresponding to the non-porous and porous vanadium pentoxide films

Sample	dc Voltage (V)	R ohm	R_{ct2} ohm	R_d ohm	Y_{03} Siemens/ (seconds)^{a3}	a_3	Y_{02} Siemens/ (seconds)^{a2}	a_2
B	-0.5	216	667	$9.18x10^3$	$317x10^{-6}$	0.613	$75x10^{-6}$	0.385
	-0.5	301	$1.4x10^3$	$31x10^3$	$402x10^{-6}$	0.592	$2.5x10^{-6}$	0.753
	-0.5	310	$1.9x10^3$	$154x10^6$	$419x10^{-6}$	0.486	$1.5x10^{-6}$	0.802
	-1.0	260	$4.6x10^3$	$616x10^6$	$58x10^{-6}$	0.573	$1.7x10^{-6}$	0.762
H	0.0	202	185	$113x10^3$	$510x10^{-6}$	0.478	$6.5x10^{-9}$	0.984
	-0.5	175	225	$1.97x10^3$	$59x10^{-6}$	0.641	$17x10^{-9}$	0.898
	-0.5	169	232	$3.81x10^3$	$40x10^{-6}$	0.665	$20x10^{-9}$	0.876
	-0.5	175	225	$5.93x10^3$	$35x10^{-6}$	0.664	$15x10^{-9}$	0.9
	-1.0	183	206	$16.2x10^3$	$84x10^{-6}$	0.582	$8.4x10^{-9}$	0.951
I	-0.5	71	320	$41x10^3$	$37x10^{-6}$	0.782	$513x10^{-9}$	0.617
	-0.5	0.871	593	$428x10^3$	$14x10^{-6}$	0.856	$18x10^{-6}$	0.351
	-0.5	93	569	$371x10^3$	$12.6x10^{-6}$	0.870	$17x10^{-6}$	0.405
	-1.0	212	716	$461x10^3$	$10x10^{-6}$	0.846	$9.2x10^{-6}$	0.535
	-1.0	215	875	$1.1x10^6$	$8.9x10^{-6}$	0.842	$8.14x10^{-6}$	0.541
N	-0.5	142	158	$5.35x10^3$	$236x10^{-6}$	0.474	$4.5x10^{-6}$	1
	-0.5	151	154	$9.73x10^3$	$191x10^{-6}$	0.508	$5.9x10^{-6}$	1
	-0.5	132	173	$58.5x10^3$	$236x10^{-6}$	0.486	$8.6x10^{-9}$	0.967
	-1.0	$68x10^{-3}$	351	$9.87x10^3$	$5.4x10^{-6}$	0.573	$459x10^{-9}$	0.967

4.2 Sol-gel prepared vanadium pentoxide thin films dip-coated at sub-zero temperature

As mentioned earlier, by dip-coating the precursor solution at a low (sub-zero) temperature, we can take advantage of the higher rate of deposition associated with this method [40]. The structure, morphology, optical and electrochromic properties of dense and porous vanadium oxide films coated at low temperature were determined and compared to those of the corresponding films deposited under room-temperature conditions. The results indicated that in the films coated at -10^0C, a residual compressive stress exists that would originate from the formation of micro-voids during the deposition. These micro-voids are preserved during the heat-treatment of the films. The micro-void morphology would favor the formation of nanostructures that would be responsible for the improved electrochromic properties of the sub-zero dip-coated films. Low-temperature coated films, heated at 450^0C for several hours, undergo

the transformation from a layered to a highly uniform nanorod structure that would be an important feature for different applications.

Effect of the sub-zero temperature deposition on the structure and morphology of the film

Vanadium pentoxide has an orthorhombic structure and crystallizes in the Pmmn space group, with the unit cell parameters: a = 11.51 Å, b = 3.563 Å, and c = 4.369 Å.

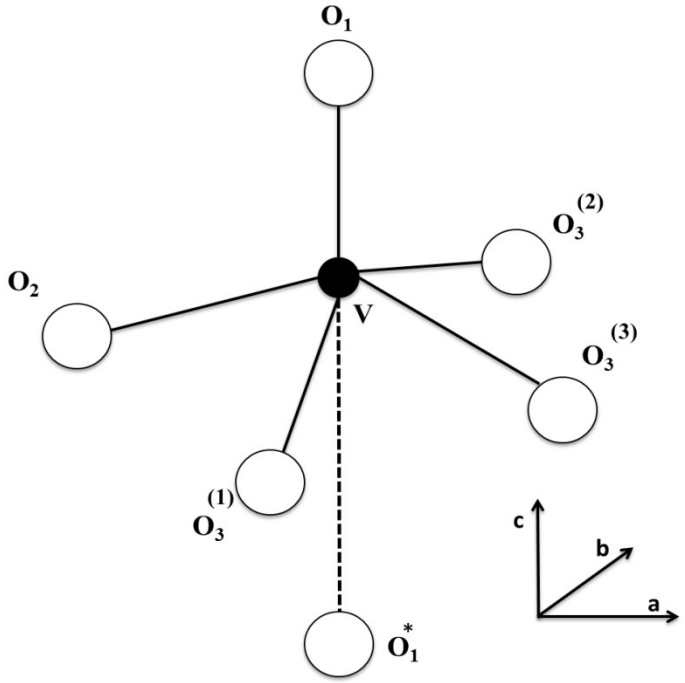

Figure 4.25: Coordination of vanadium with oxygen in vanadium pentoxide.

The layered structure of orthorhombic V_2O_5 is built up of edge-sharing VO5 square pyramids. As shown in Figure 4.25, vanadium atoms form five bonds with the atoms of oxygen: one with O_1 atoms, one with O_2 atoms and three with O_3 a toms. The shortest bond is the one with O_1 (1.585 Å) and this oxygen is usually called the "vanadyl" oxygen. The O_2 oxygen is called the `bridging` oxygen and the O_3 oxygen atoms are called "chain" oxygen. The layers are held together by weak V- O_1^* bonds in the crystallographic c direction.

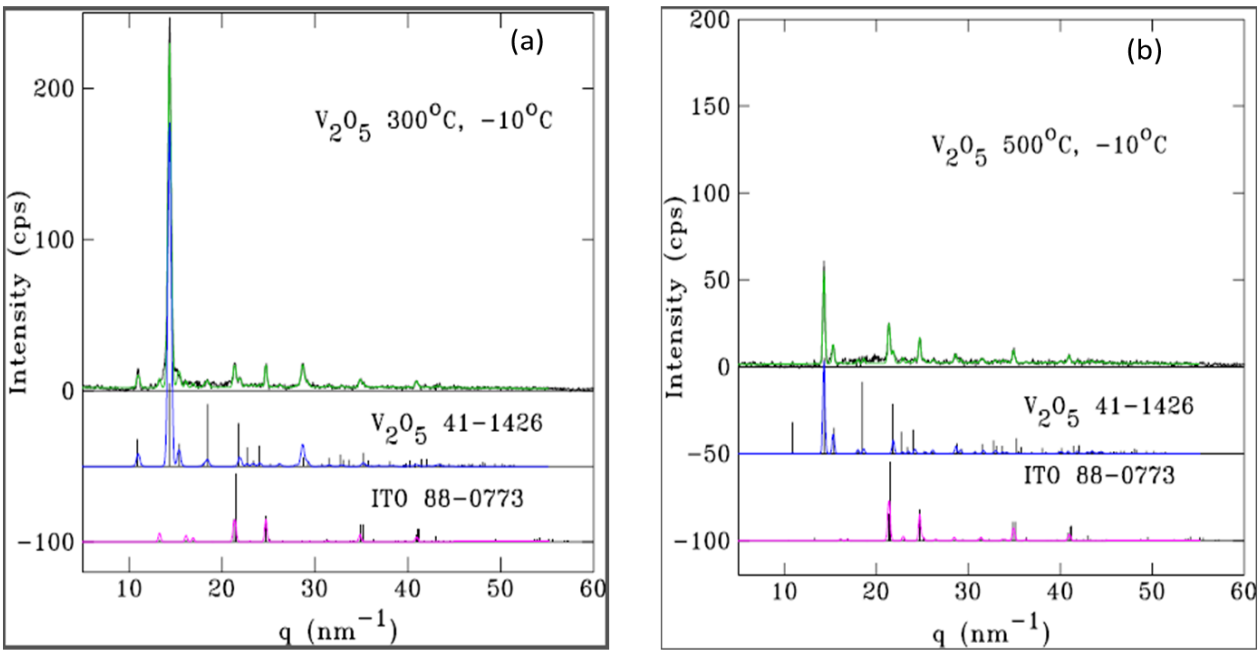

Figure 4.26: XRD pattern of the vanadium oxide films dip-coated at -10^{0}C and annealed at 300^{0}C (sample D) (a) and 500^{0}C (sample H) (b). X-ray diffraction signal of an orthorhombic V_2O_5 film (ICDD 41-1426) on an ITO covered glass substrate, annealed at 500^{0}C for one hour

The signal from the glass substrate has been subtracted. Below the JCPDS reference patterns are shown. The fit (red line) includes the contributions from V_2O_5 and ITO to the signal.

Figure 4.26 shows the XRD pattern of the sub-zero dip-coated V_2O_5 film, annealed for one hour in air at 300 and 500^{0}C, respectively. The data are shown as a function of modulus of the scattering vector, $q=4\pi\lambda^{-1}\sin\theta$, where 2θ is the scattering angle. The signals include the contributions from the V_2O_5 film and the ITO substrate. Reference patterns from the JCPDS database are indicated by the vertical lines. Based on a fit to the data (red line), the dimensions of the orthorhombic unit cell for the sub-zero dip-coated films are shown in Table 4.6.

Table 4.6 Crystallographic data corresponding to sub-zero dip-coated vanadium pentoxide films

Sample	Deposition temperature	a, nm	b, nm	c, nm	Unit cell volume, nm^3	Size, nm
300^0C	-10^0C	1.1477	0.3574	0.4385	0.1799	14.54
	RT	1.1440	0.3592	0.4375	0.1798	12.27
500^0C	-10^0C	1.1478	0.3521	0.4380	0.1770	23.14
	RT	1.1454	0.3608	0.4387	0.1813	23.07
Literature data		1.1516	0.3565	0.4372	0.1795	

In general, we find that the lattice parameters of the vanadium oxide crystallites are close to the literature values. However, the parameter a is found to be somewhat larger in the film deposited at -10C and annealed at 500^0C, than in the film dip-coated at room-temperature and annealed under the same conditions (1.1477 nm, compared to 1.1454 nm), while b appears to be shorter (0.3521 nm compared to 0.36087 nm). The smallest unit cell volume corresponds to the sub-zero deposited film, annealed at 500^0C (0.1770 nm^3. After annealing at 300^oC, the crystallite size estimate by the Scherrer equation is 15 nm, whereas upon annealing at 500^oC the crystals grow to 23 nm.

In order to account for the changes observed in the crystallographic data, the Raman spectra of the film dip-coated at -10^0C have been investigated. Figure 4.27 shows the Raman spectrum of the film dip-coated at -10^0. The positions and assignments of the Raman bands corresponding to the sub-zero and room-temperature dip-coated samples are shown in Table 4.7. The point symmetry group of V_2O_5 is D_{2h}.

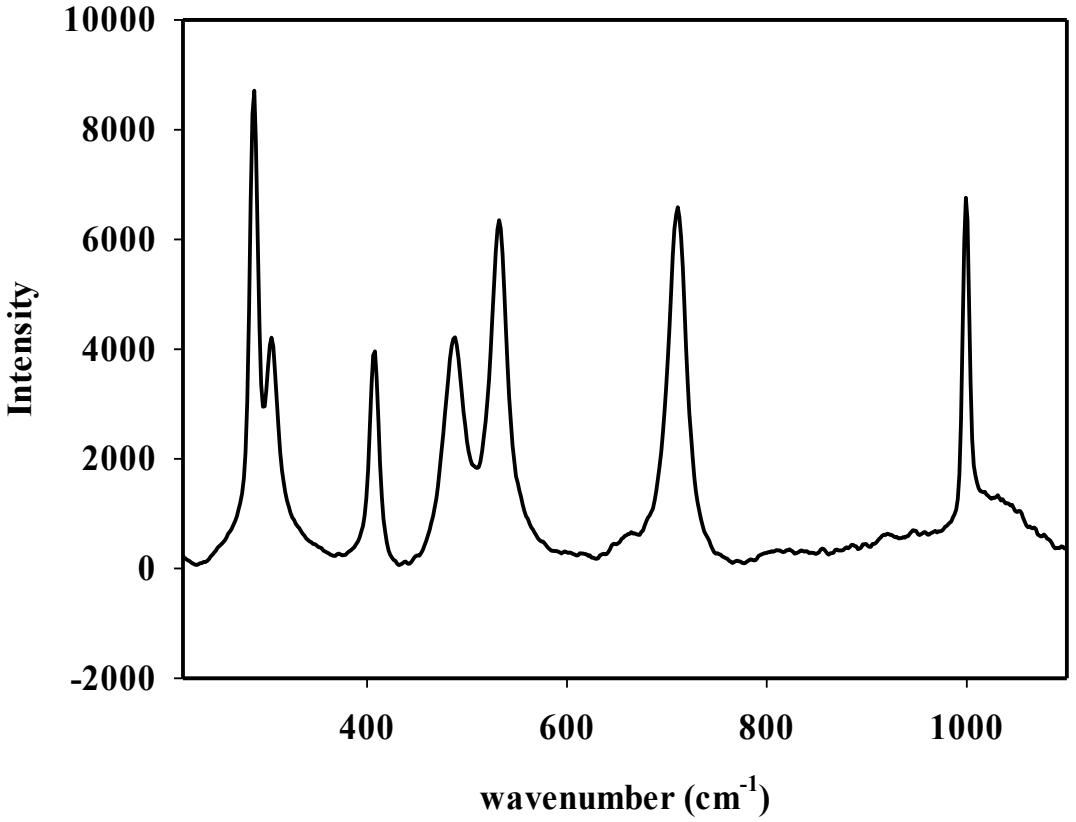

Figure 4.27: Raman spectrum of the V_2O_5 film dip-coated at -10^0C and annealed at 500^0C (sample H)

Table 4.7 Position of the Raman bands in the spectra corresponding to the sub-zero- and room-temperature dip-coating.The Raman bands were assigned according to references [15,16].

Position of Raman bands (cm^{-1})			Assignment
RT[a]	SZT[b]	$\Delta\nu^{*}$ (cm^{-1})	
997.49	997.96	+0.47	ν(terminal O)
708.44	711.26	+2.82	ν(V2-O)
528.15	532.16	+4.01	ν(V3-O)
484.75	486.71	+1.96	δ(V-O-V)
406.06	408.03	+1.97	δ(V=O)
303.32	303.66	+0.34	-
283.97	286.95	+2.98	δ(V=O)

[a]room - temperature dip-coated and annealed at 500^0C
[b]sub-zero temperature dip-coated and annealed at 500^0C
*SZT-RT

Table 4.7 shows that all the Raman bands of the low-temperature dip-coated samples are at higher wave numbers than those of the RT-coated samples annealed at the same temperature, i.e., 500^0C. The most sensitive bands (the most affected by the temperature of the coating) are the V2-O and V3-O stretching bands and the vanadyl bending band. Both XRD and Raman spectroscopy results indicate that a residual compressive stress (or strain) exists in the sub-zero dip-coated V_2O_5 film. This stress may originate in a difference in the thermal expansion coefficients of the thin film and its substrate (thermal mismatch stress) and/or in the grain structure, fabrication process etc. In addition, the stress is possibly due to non-uniformity through the depth, for example the formation of micro voids when by-products may escape as gases. Due to the slow diffusion of atoms at low-temperature, there remain empty spaces in the film that results in an intrinsic stress. The micro voids formed during the low-temperature deposition can be clearly seen in the SEM images of the films (Figure 4.28 and Figure 4.29). Interestingly, micro voids can be seen in the micrographs corresponding to both the annealed and extracted films, reinforcing the idea that they are formed during the dip-coating process.

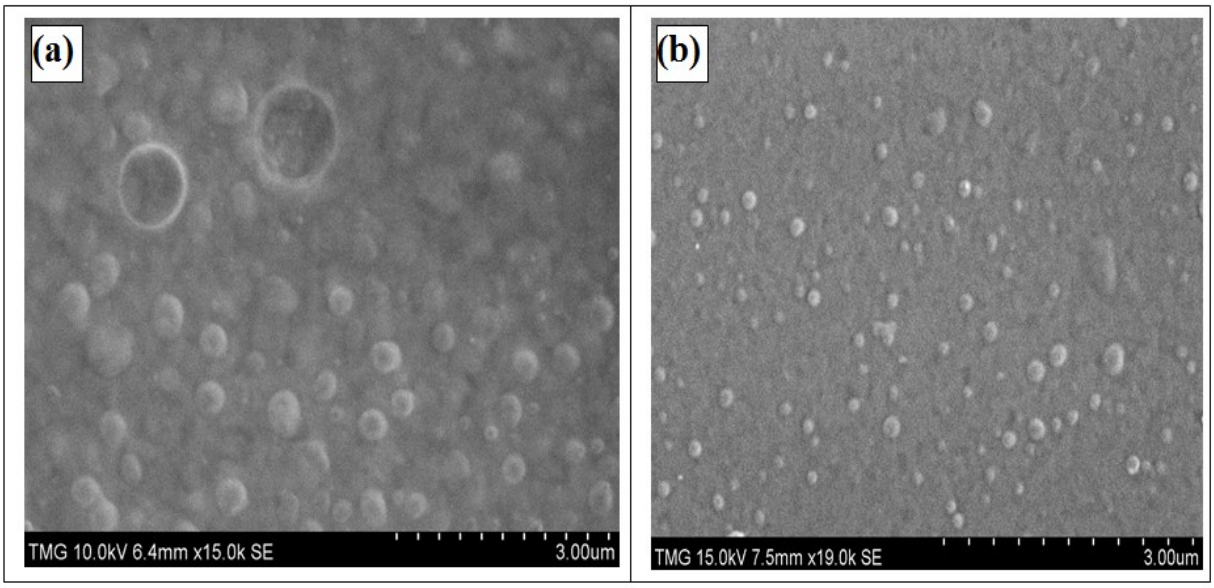

Figure 4.28: SEM image of a low-temperature coated dense film (a) and, image of the RT dip-coated film (annealed at 300°C, sample D)(b)

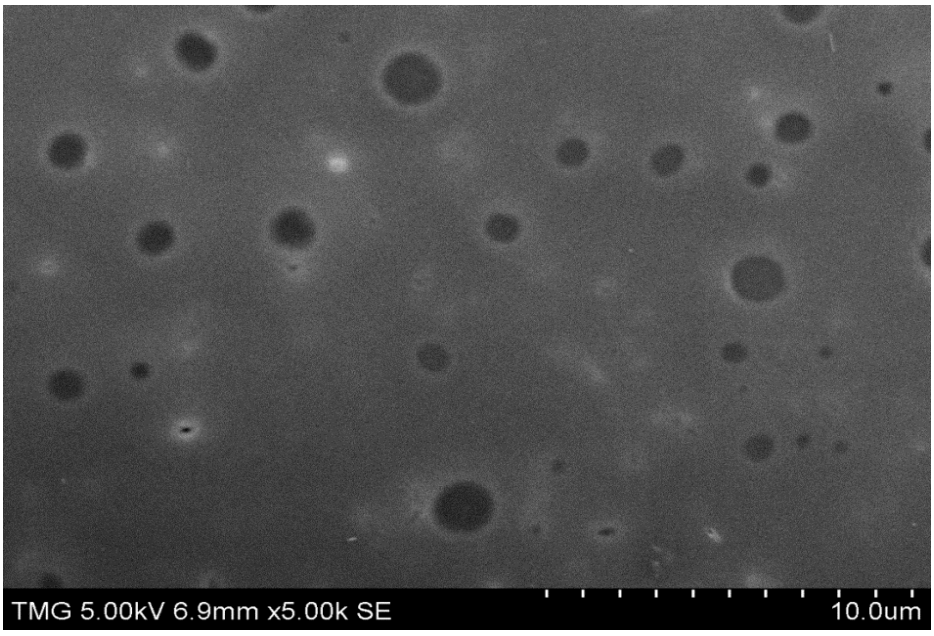

Figure 4.29: SEM image of the vanadium oxide film obtained by dip-coating at -10^0C (templated with PS microspheres and extracted with THF (sample I)

However, after heating the sub-zero coated film to 450^0C for 3 hours, the formation of nanorods can be observed as it has been noted in the case of the room-temperature coated films.

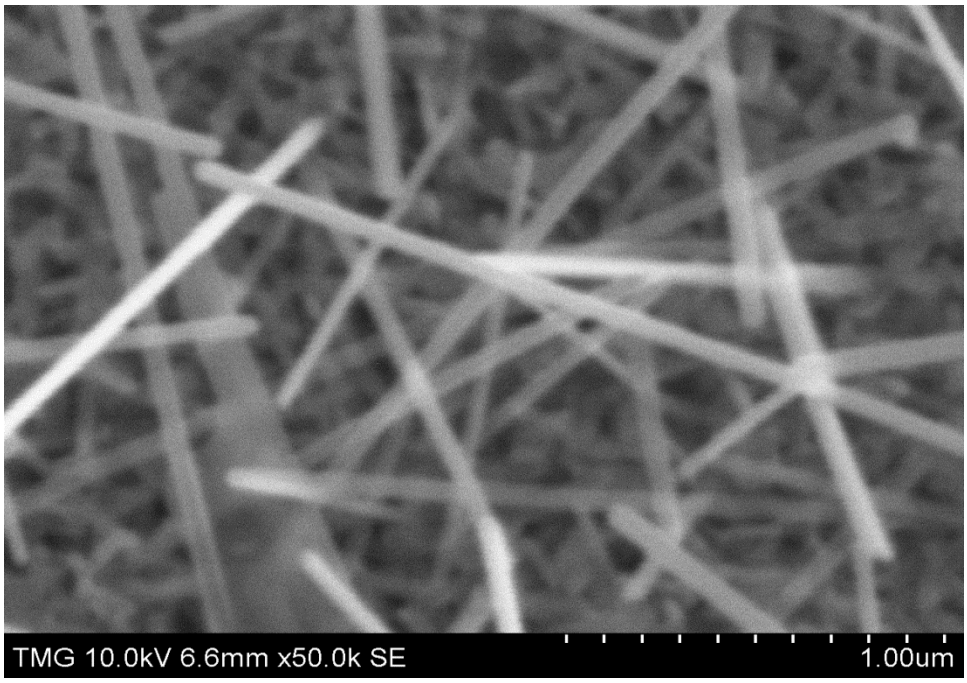

Figure 4.30: SEM image of the V_2O_5 nanorod film dip-coated at -10^0C and annealed at 450^0C for 3h (templated with the triblock copolymer (sample G)

The SEM image in Figure 4.30 shows that, indeed, the nanorods, formed by the extended annealing of the low-temperature deposited film, are more uniform than those formed from a layered film, dip-coated at room temperature. This is a significant result as it opens the door to the preparation of uniform nanorods with important future applications.

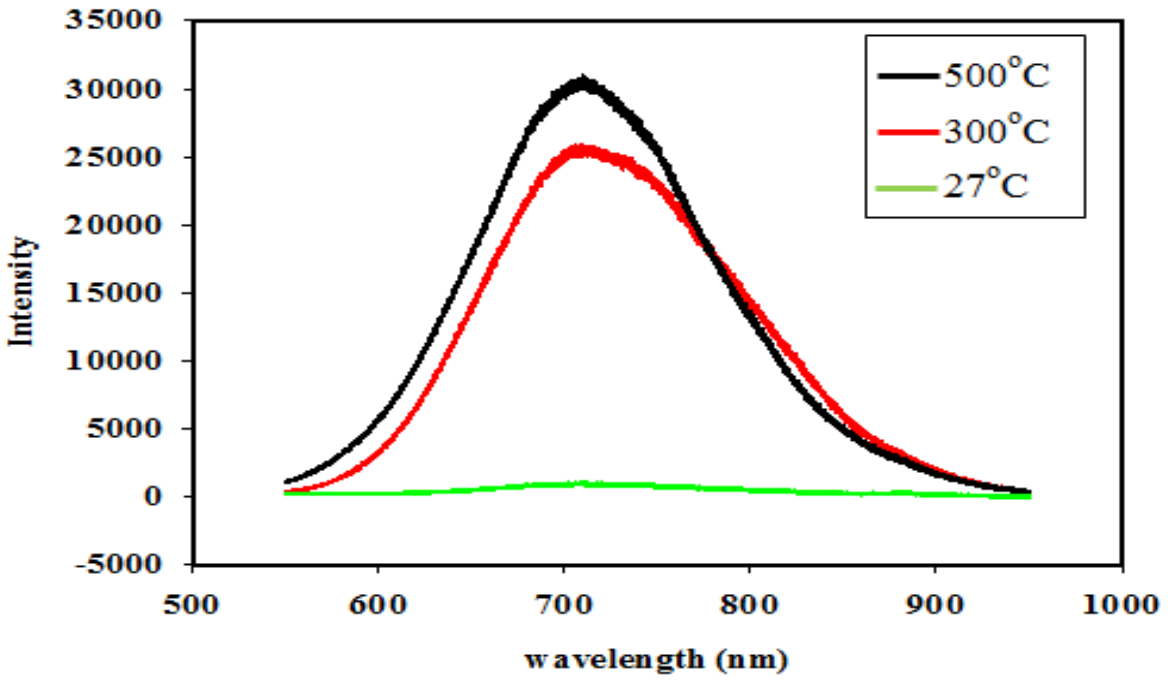

Figure 4.31: Photoluminescence spectra of the sub-zero temperature dip-coated film (a) and of the RT deposited film (b), both annealed at 27 (green), 300 (red), and 500^0C (black), respectively

The results show that the sub-zero temperature deposition of the V_2O_5 films significantly varied its photoluminescence properties, as seen in Figure 4.31.

Figure 4.31(a), corresponding to the sub-zero deposited film, displays no PL bands at room temperature and the band around 750 nm, in the case of the films annealed at 300 and 500^0C, have almost the same intensity. The second band is missing, possibly, because of less structural defects such as vacancies in the crystal lattice, in the low-temperature deposited film.

The PL spectrum corresponding to the room-temperature coated film (Figure 4.7 (b)), shows a shift of the band, from 760 to 705 nm when the film is heated to 300°C and the intensity of the emission at 700 nm is considerably higher than when the film was heat-treated at 500°C in air. It can be seen that the intensity of the second PL band, around 880 nm, is slightly increasing with the annealing temperature. Taking into account the phase change observed at 500°C, the high

intensity of the visible light emission has been explained by oxygen vacancies or/and the V^{4+} defects that could appear during the formation of the nanorods [30].

Mechanism of the formation of nanorods by high-temperature annealing

In order to investigate the mechanism of transformation of the layered structure in nanorods, in the case of the sub-zero temperature dip-coated films, the time of annealing was varied between 1 and 3 hours. The SEM images of the resultant films are shown in Figure 4.32. The figure shows that, after only one hour heating, the film still shows the micro voids, after two hours, some star-like structures are formed that will lead after an extended heating to the formation of nanorods.

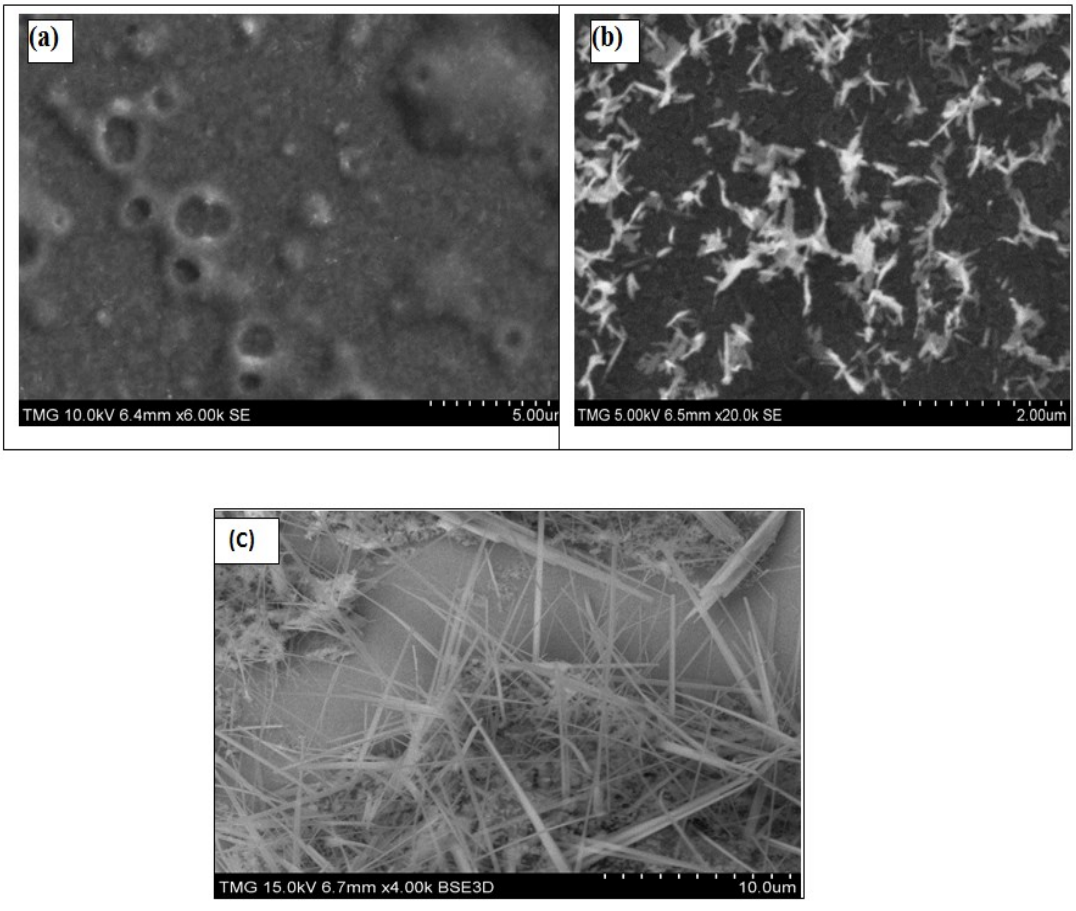

Figure 4.32: SEM image of the film templated with PS microspheres (600 nm) and annealed at 450^0 C for 1h (sample I) (a) 2 hours (b) and 3 hours) (c)

Effect of the sub-zero temperature deposition on the electrochromic properties

In this section, we compare the electrochromic (EC) properties, namely, the coloration efficiency and diffusion coefficients of the sub-zero coated films with those of the films, deposited under the same conditions at room-temperature, thoroughly investigated in our previous work [41]. The EC measurements were carried out both on the dense films and on those fabricated by using structure-directing molecules, that is, on "templated films". The intercalated charge (Q) and the coloration efficiency (CE) in the Visible (600 nm) and Near-Infrared (843 nm) for the dense, and templated films are shown in Table 4.8 and 4.9, respectively.

Before performing the EC measurements, the thickness of the films were determined by AFM.

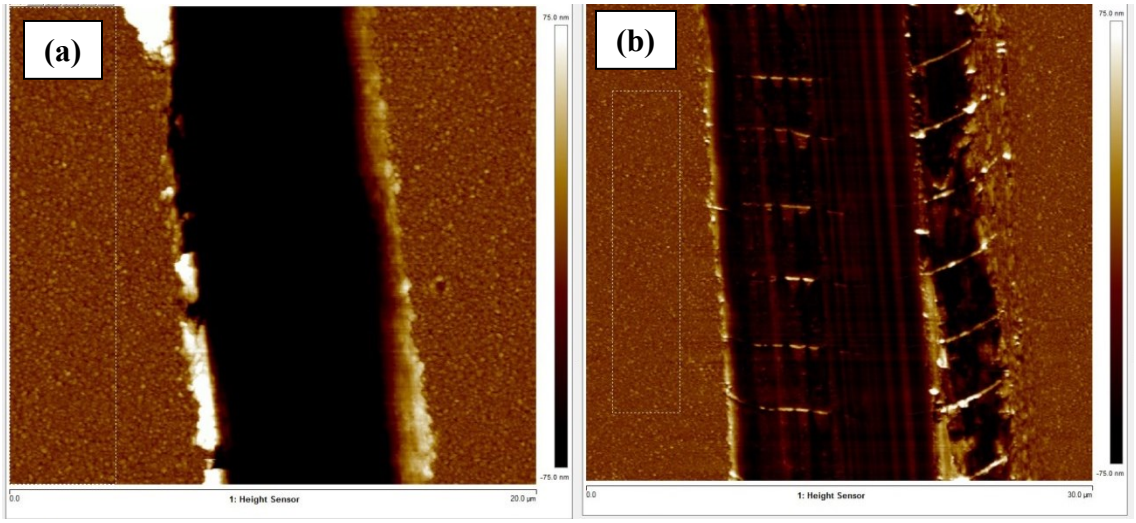

Figure 4.33: AFM images of scratched films coated at -10^{0}C (a) and room temperature (b)

The thickness and the roughness of both films were measured by scratched films, by using AFM measurements (Figure 4.33). The results indicated that, indeed, the thickness of films dip-coated at -10^{0}C, under precisely the same conditions, is almost twice, compared with the RT- deposited films (around 130 versus 66 nm, respectively). This result is in agreement with the data found for the sub-zero coated ZnO films and accounted for by a higher deposition rate because of the increased viscosity of the coating solution at low-temperatures [40]. The roughness of the films

was found quite high, around 63 nm, compared to 54 nm corresponding to the RT-deposited film.

Figure 4.34(a) shows a typical voltammogram of a sub-zero deposited (and annealed at 500^0C) film and Figure 4.34(b) illustrates the optical modulation corresponding to the same film, in the visible (red) and near-infrared (green) range of the spectrum, respectively. The voltammogram corresponds to the film-stabilized electrochemically, after 25 cycles at a scan rate of 30 $mV.s^{-1}$ and shows a strong peak at -0.10 V corresponding to the lithium intercalation. Weaker peaks are seen at 0.20, 1.20 and 0.50 V. Compared to the room-temperature coated film, the voltammogram has less peaks and they appear to be shifted.

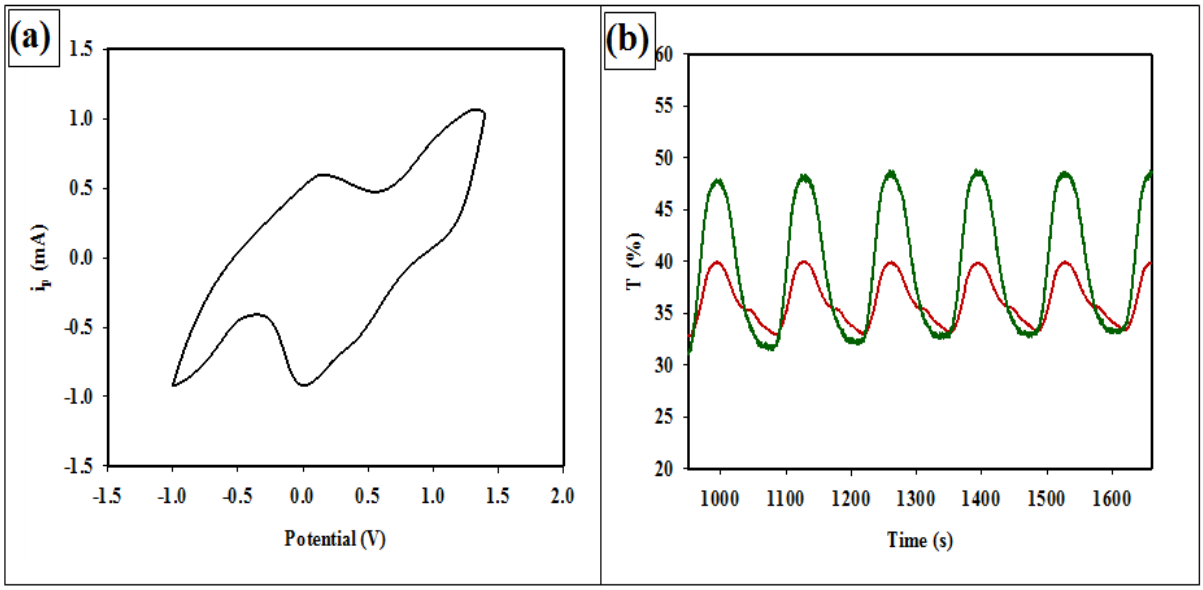

Figure 4.34: Cyclic voltammogram (a) and optical modulation (b) corresponding to sample G. The modulation is shown at 600 nm (red) and at 843 nm (green)

Table 4.8 Coloration efficiency (CE) of the sub-zero coated dense films, subsequently annealed at different temperatures

Sample	Temperature of drying/annealing (^{o}C)	Q (mC)		CE (cm^2/C) (600 nm)		CE (cm^2/C) (843 nm)	
		RT	SZT	RT	SZT	RT	SZT
B	RT	9	14	19	32	3	13
D	300^{o}C	18	16	28	4	28	44
G	450^{o}C	23	19	22	23	51.9	73
H	500^{o}C	13	19	24	53	68	38

The coloration efficiency of the sub-zero (SZT) coated films are compared with those of the RT-deposited films. The CE values shown in Table 4.8 are invariably higher, especially in the NIR range, than those corresponding to the room-temperature deposited films and the same tendency is shown by the data given in Table 4.9 for the templated films. However, in this case, the CE values are not significantly increased. The high values of the diffusion coefficient found for the templated films confirm the porous nature of the films. The largest CE, that is, 73 cm^2/C, was found for the SZT- coated film, annealed at 450^{0}C for 1 hour (sample C), while for the RT-deposited films, the highest CE is reached for the film annealed at 500^{0}C (sample D). For the SZT-coated films, annealed at 300^{0}C, the higher CE may be due to the presence of micro-voids. For temperatures of 450 and 500^{0}C, respectively, the formation of uniform nanorods may account for the enhanced CE values.

In the case of porous films (Table 4.9), the values of the coloration efficiency are lower than for the dense films (Table 4.8). Except for the nanorod film (sample H) that results from the PS-templated film that are particularly rich in micro voids, the CE values of the low-temperature dip-coated films are comparable with those previously calculated for the RT deposited films.

Table 4.9 Coloration efficiency (CE) and diffusion coefficient of Li^+ in porous films prepared with structure directing agents

Sample	Templated film	CE (cm^2/C) (843 nm)		D (cm^2/s)	
		RT	SZT	RT	SZT
O	Copolymer (20%)	28	35	$2.8x10^{-10}$	$2.9x10^{-10}$
I	PS (600nm)	33	57	$8.3x10^{-11}$	$1.5x10^{-10}$

Electrical impedance spectroscopy

The equivalent circuit used to obtain the fitting is shown in Figure 4.35.

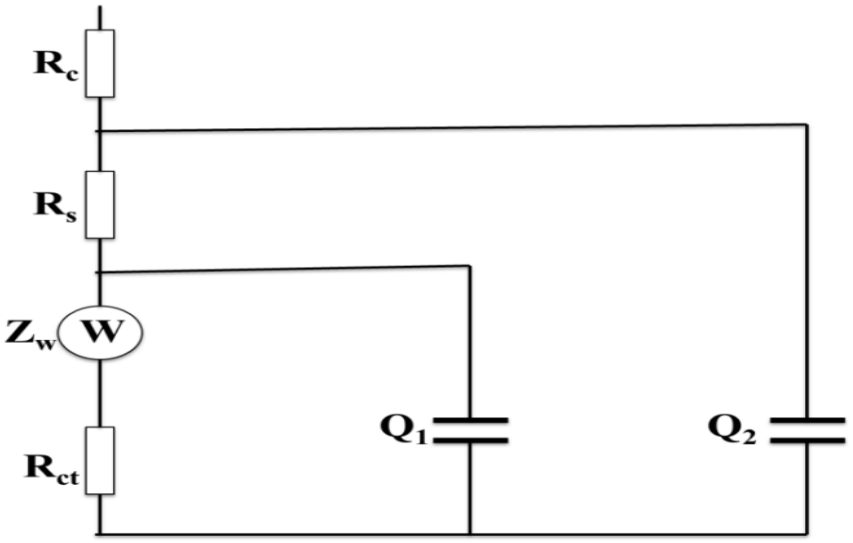

Figure 4.35: Equivalent circuits used to obtain the fitting parameters [68]

In Figure 4.35 R_c is the resistance of the electrolyte, R_s is the resistance representing the adsorption of the lithium ion into the oxide film, R_{ct} is associated with the charge transfer process occurring at the cathode / electrolyte interface, and Z_W is the Warburg impedance associated with the diffusion of the lithium ion through the oxide film. Q_1 and Q_2 are constant phase elements.

The electrochemical impedance spectra (Nyquist plots) corresponding to the copolymer-templated samples (see Table 2.1b), subjected to dc potentials of -0.5 and -1.0 V, respectively, are shown in Figure 4.36.

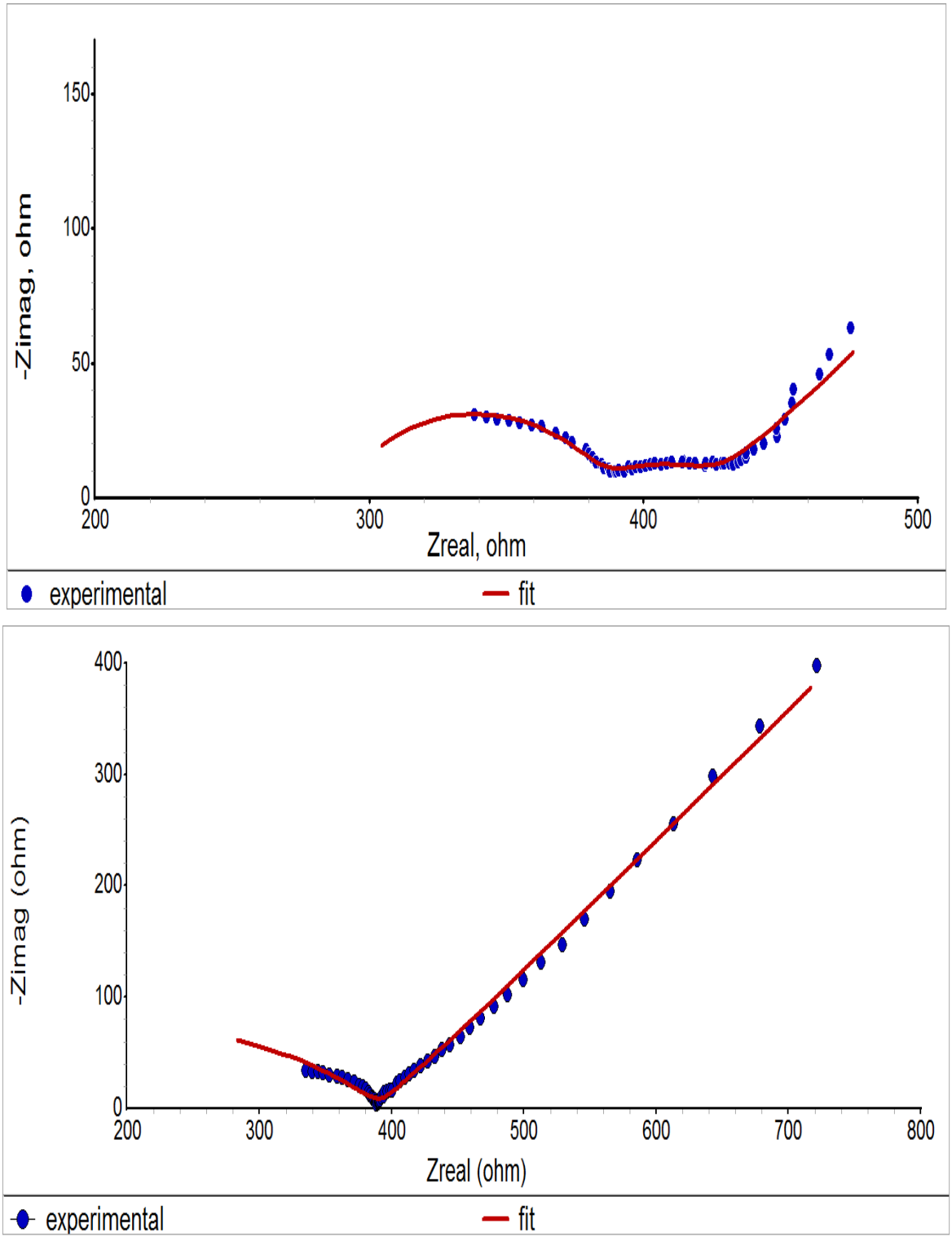

Figure 4.36: Nyquist plots corresponding to the tri-block copolymer templated sample subjected to potentials of -0.50 V (top) and -1.0 V(bottom), respectively

When compared to the spectrum measured at -0.5 V, the curve measured at -1.0 V is displaced towards lower resistances – associated with faster kinetics.

The measured electrochemical impedance spectra at different electrode potentials were analyzed. The results show that the Nyquist plot impedance spectra consist of two medium frequency depressed arcs and a low frequency straight line. The low frequency line with a phase angle of 45^{o} corresponds to the diffusion of lithium ion through the vanadium oxide phase.

In Table 4.10, the charge transfer resistance values found for the sub-zero dip-coated samples are compared with those of the room-temperature deposited samples. The charge transfer resistance (R_{ct2}) is the most important parameter related to the V^{5+}/V^{4+} reduction process occurring at the electrolyte/vanadium oxide film. Table 4.10 shows the values found by curve fitting for the dense and porous samples as well as their dependency on the applied dc potential.

Table 4.10 Fitting parameters corresponding to the sub-zero temperature dip-coated films

Sample	dc Voltage (V)	R_c ohm	R_s ohm	W $S^*s^{0.5}$	R_{ct} ohm		Q_1 S^*s^a	a_1	Q_2 S^*s^a	a_2
					SZT	RT				
H	-0.5	378	91	$3.6x10^{-3}$	246	225	$82x10^{-6}$	$700x10^{-3}$	$69x10^{-9}$	$809x10^{-3}$
	-0.7	343	123	$482x10^{-6}$	1158	-	$135x10^{-6}$	$650x10^{-3}$	$61x10^{-9}$	$817x10^{-3}$
	-1.0	$43x10^{-9}$	502	$42x10^{-6}$	15004	206	$49x10^{-6}$	$804x10^{-3}$	$7.1x10^{-6}$	$303x10^{-3}$
	-1.2	$5x10^{-6}$	493	$28x10^{-6}$	307	-	$55x10^{-6}$	$820x10^{-3}$	$1.7x10^{-6}$	$514x10^{-3}$
N	-0.5	289	97	$12x10^{-3}$	40	173	$410x10^{-6}$	$594x10^{-3}$	$743x10^{-9}$	$720x10^{-3}$
	-1.0	36	357	$1.1x10^{-3}$	101	351	$768x10^{-6}$	$678x10^{-3}$	$1.1x10^{-6}$	$475x10^{-3}$
	-1.2	257	155	$764x10^{-9}$	110	-	$469x10^{-6}$	$624x10^{-3}$	$645x10^{-9}$	$697x10^{-3}$

In Table 4.10, the charge transfer resistance (R_{CT}) values of the low-temperature deposited films (SZT) are compared to those corresponding to the films coated at room temperature (RT). Table 4.10 shows that for sample H (nanorods obtained from the dense film), R_{CT} is increasing significantly with the applied dc potential, while for the porous sample (N), R_{CT} is increasing only slightly. Compared with the RT- deposited samples, R_{CT} values appear to be larger for the dense film and significantly lower for the porous film, indicating that the intercalation of lithium

ions is easier in the porous films. This result is in agreement with our previous work on dense and porous V_2O_5 films.

Chapter 5

5 Conclusion and outlook

5.1 Concluding remarks

V_2O_5 dense and porous films have been prepared through a sol-gel method. Films were deposited on indium-tin-oxide substrates by dip-coating at both room- and sub-zero temperatures (-10^0C). Polystyrene microspheres or a non-ionic polymer surfactant (Pluronic P-123) were used to create porosity in the vanadium pentoxide thin films in order to enhance their electrochromic properties.

In the first part of this work, the study of the room-temperature coated films has confirmed that by using template materials, the morphology of the vanadium pentoxide film can be controlled and new nanostructures can be created. We have shown that the optical modulation of the V_2O_5 films strongly depends on the number of the deposited layers and, hence the thickness of the films. The coloration efficiencies of the dense films in the near-infrared region of spectrum was found around 68 cm^2/C, when the sample was annealed at 500° C, which is considerably higher than those found in the literature (in the range of 12-14 cm^2/C).

We have observed that vanadium pentoxide films, with or without templating materials, when heated at around 450^0C, show a morphological transformation from a layered to a nanorod structure showing improved electrochromic properties, especially in the near infrared region.

The electrochromic performance of the nanorods prepared through the thermal treatment was found to be superior to that of the vanadium pentoxide with the layered structure, especially in the near-infrared region, demonstrating their potential for different electrochromic applications.

The diffusion coefficient corresponding to the nanorods morphology of the vanadium oxide was found considerably higher than that corresponding to the layered structure (7.95×10^{-11}), indicating different topological lithium intercalation sites. The highest value corresponds to the sample with the highest concentration of triblock copolymer, having a larger porosity left behind after its removal. In the films coated on polystyrene colloidal crystals, the lithium diffusion coefficients were found higher as compared to the dense film. SEM images have shown that

annealing the films at 450-500^0, even without structure-directing molecules, leads to the transformation of the layered structure into a nanorod structure. The electrochromic properties, especially the coloration efficiency of the nanorod films are considerably improved in the near-infrared region of the spectrum. The Raman spectra give evidence of the crystalline structure of the nanorods and the photoluminescence spectra show a high intensity of the visible light emission. The yield of nanorods can be controlled through the number of deposited layers. The electrochromic properties of the vanadium oxide nanorods proved to be different from the layered film: the cyclic voltammogram displayed additional redox peaks indicating a good reversibility of the intercalation. The features of the curves point toward a multi-step lithiation process. The optical modulation was found to be larger in the near-infrared region than in the visible, giving surprisingly high coloration efficiencies. Electrical impedance spectroscopy measurements indicated low values of the charge transfer resistance for the porous films as well as for the nanorod films, in agreement with the high coloration efficiency and the diffusion coefficient.

In the second part of this work, vanadium oxide thin films have been prepared by a sub-zero temperature dip-coating method. Structural properties as well as Raman spectroscopy and the morphologic characteristics have indicated the presence of a residual compressive stress in the films dip-coated at -10^{0}C. The stress is believed to exist due to the formation of micro-voids during the deposition process, micro-voids that are preserved during the heat-treatment of the films. The micro-voids are pores that provide additional sites for the intercalation of lithium ions in both dense and porous films, and their presence may explain the enhanced electrochromic properties of the vanadium oxide films. The results indicated that, indeed, the thickness of films dip-coated at -10^{0}C, under precisely the same conditions, is almost twice, compared with the RT-deposited films (around 130 versus 66 nm, respectively). This result is in agreement with the data found for the sub-zero coated ZnO films and accounted for by a higher deposition rate because of the increased viscosity of the coating solution at low-temperatures. The roughness of the films was found quite high, around 63 nm, compared to 54 nm corresponding to the RT-deposited film. The coloration efficiencies in the near infrared region of the PS microsphere-templated films were improved for the samples coated at sub-zero temperature as compared to the same sample coated at room-temperature. The voltammogram of the film annealed at 450°C, shows a strong peak at -0.10 V corresponding to the lithium intercalation. Compared to the

room-temperature coated film, the voltammogram has less peaks and they appear to be shifted. Regarding the vibrational spectrum, it is found that all the Raman bands of the low-temperature dip-coated samples are at higher wave numbers than those of the RT-coated samples. Both the crystallographic and Raman data indicate the presence of a stress in the film.

Highly uniform nanorods, interesting for future applications such as field emission displays, interconnects, etc. have been obtained by annealing at 450^0C of the sub-zero coated films. The transformation of the layered film into the nanorods is thought to happen slower and through a mechanism that seems to be different from the transformation of room-temperature deposited films.

For both techniques mentioned above, the charge transfer resistance (R_{CT}) values appear to be larger for the dense film than for the porous film, indicating that the intercalation of lithium ions is easier in the porous films.

The method suggested in this work is a straightforward way to prepare vanadium pentoxide nanorods for EC applications.The fabrication method proposed is simple and it may be used for deposition on larger surfaces as well.

5.2 Possible extension of present work

There would be several avenues possible for an extension of the present work. First, the improved electrochromic properties of the vanadium oxide films obtained in this study can make them a good candidate for EC applications, especially in the NIR spectral range. Secondly, our ability to fabricate by the simple sol-gel process the nanorod structures as well as the highly porous ones by templating methods can be exploited further in composites involving vanadium pentoxide and other EC materials such as WO_3 or MoO_3. A mixture of V_2O_5 in nanorod structure with WO_3 will result in a highly porous EC film, susceptible to exhibit a higher EC performance, especially regarding the response times and the modulation capacity both in the VIS and the NIR ranges. Another possible extension would be the perfecting of the fabrication of uniform nanorods of V_2O_5 for potential applications as interconnects or field emission displays as mentioned previously.

References

1. CK. Chan, H. Peng, RD. Twesten, K. Jarausch, XF. Zhang, and Y. Cui, *Fast, completely reversible li insertion in vanadium pentoxidenanoribbons*, Nano Lett. **7**, 490 (2007).
2. J. Scarminio, P. R. Catarini, A. Urbano, R. V. Gelamo, F. P. Rouxinol, and M. A. Bica de Moraes, *Li diffusion and electrochromism in amorphous and crystalline vanadium oxide thin film electrodes*, J. Braz. Chem. Soc. **19**, 788 (2008).
3. K. Jeyalakshmi, and G. Muralidharan, *Role of annealing duration on the microstructure and electrochemical performkance of β-V_2O_5 thin films*, Philos. Mag. **94**, 946 (2014).
4. Q. H. Wu, A. Thissen, W. Jaegermann, and M. Liu, *Photoelectron spectroscopy study of oxygen vacancy on vanadium oxides surface*, Appl. Surf. Sci. **236**, 473 (2004).
5. M.S. Whittingham, *Lithium batteries and cathode materials*, Chem. Rev. **104,** 4271 (2004).
6. L.A.L. de Almeida, G.S. Deep, A.M.N. Lima, I.A. Khrebtov, V.G. Malyarov, and H. Neff, *Modeling and performance of vanadium–oxide transition edge microbolometers*, Appl. Phys. Lett. **85**, 3605 (2004).
7. L. Krusin-Elbaum, D.M. Newns, H. Zeng, V. Derycke, J.Z. Sun, and R. Sandstrom, *Room-temperature ferromagnetic nanotubes, controlled by electron or hole doping*, Nature **431**, 672 (2004).
8. Israel E. Wachs, *Catalysis science of supported vanadium oxide*, Dalton Trans. **42,** 11762 (2013).
9. B.M. Weckhuysen, and D.E. Keller, *Chemistry, spectroscopy and the role of supported vanadium oxides in heterogeneous catalysis*, Catal. Today **78**, 25 (2003).
10. X.J. Wang, H.D. Li, Y.J. Fei, X. Wang, Y.Y. Xiong, Y.X. Nie, and K.A. Feng, *XRD and Raman study of vanadium oxide thin films deposited on fused silica substrates by RF magnetron sputtering*, Appl. Surf. Sci. **177**, 8 (2001).
11. G. Silversmith, H. Poelman, R.D. Gryse, Surf. Interface Anal. **36**, 1163 (2004).
12. Benmoussa, E. Ibnouelghazi, A. Bennouna, and E.L. Ameziane, *Structural, electrical and optical properties of sputtered vanadium pentoxide thin films*, Thin Solid Films **265**, 22 (1995).

13. Se-Hee Lee, H. M. Cheong, P. Liu, and C. E. Tracy, *Improving the durability of amorphous vanadium oxide thin-film electrode in a liquid electrolyte*, Electrochemical and Solid-State Letters **6**, A102 (2003).
14. J. G. Fang, Z. L. Liu, Y. Wang, Y. H. Liu, and K. L. Yao, *Synthesis and structural, electrochromic characterization of pulsed laser deposited vanadium oxide thin films*, Journal of Vacuum Science and Technology A **19**, 887 (2001).
15. C. V. Ramana, O. M. Hussain, B. Srinivasulu Naidu, and P. J. Reddy, *Spectroscopic characterization of electron-beam evaporated V_2O_5 thin films*, Thin Solid Films **305**, 219 (1997).
16. C. Julien, J. P. Guesdon, A. Gorenstein, A. Khelfa, and I. Ivanov, *The influence of the substrate material on the growth of V_2O_5 flash-evaporated films*, Appl. Surf. Sci. **90**, 389 (1995).
17. H. Groult, E. Balnois, A. Mantoux, K. L. Van, and D. Lincot, *Two-dimensional recrystallisation processes of nanometric vanadium oxide thin films grown by atomic layer chemical vapor deposition (ALCVD) evidenced by AFM*, Appl. Surf. Sci. **252**, 5917 (2006).
18. A. Bousidi, N. Benramdane, A. Nakrela, C. Mathieu, B. Khelifa, R. Desfeux, and A.D. Costa, *Characterization of Electrochromic Vanadium Pentoxide Thin Films Prepared By Spray Pyrolysis*, Mater. Sci. Eng. **95**, 141 (2002).
19. D. Vernardou, *State-of-the-art of chemically grown vanadium pentoxide nanostructures with enhanced electrochemical properties,* Adv. Mater. **4**, 798 (2013).
20. Y. Wang, and G. Z. Cao, *Synthesis and enhanced intercalation properties of nanostructured vanadium oxides*, Chem. Mater. **18**, 2787 (2006).
21. C.O. Dwyer, V. Lavayen, MA. Santa Ana, E. Benavente, G. González, and CM Sotomayor Torres, *Anisotropic vanadium oxide nanostructured host matrices for lithium ion intercalation*, Res. Lett. Phys. Chem. **2007**, 32528 (2007).
22. H. J. Muhr, F. Krumeich, U.P. Sch″onholzer, F. Bieri,M. Niederberger, L. J. Gauckler, and R. Nesper, *Vanadium oxide nanotubes – a new flexible vanadate nanophase*, Adv. Mater. **12**, 231 (2000).
23. G. R. Patzke, F. Krumeich, and R. Nesper, *Oxidic nanotubes and nanorods -anisotropic modules for a future nanotechnology*, Angew. Chem. Int. Ed. **4**, 5000 (2002).

24. F. Krumeich, F. Muhr, M. Niederberger, F. Bieri, B. Schnyder, and R. Nesper, *Morphology and topochemical reactions of novel vanadium oxide nanotubes*, J. Am. Chem. Soc. **121**, 8324 (1999).
25. F. Sediri, F. Touati, and N. Gharbi, *One-step hydrothermal way for the synthesis of vanadium oxide nanotubes containing the phenyl propyl amine as template obtained via non-alkoxide route*, Mater. Lett. **61**, 1946 (2007).
26. A. Liu,M. Ichihara, I. Honma, and H. Zhou, *Vanadium oxide nanotubes: synthesis and template-related electrochemical properties*, Electrochem. Commun. **9**, 1766 (2007).
27. X. Chen, X. Sun, and Y. Li, *Self-assembling vanadium oxide nanotubes by organic molecular templates*, Inorg. Chem. **41**, 4524 (2002).
28. N. Pinna, M Willinger, K. Weiss, J. Urban, and R. Schlögl, *Local structure of nanoscopic materials: V2O5 nanorods and nanowires*, Nano Lett. **3**, 1131 (2003).
29. K. Takahashi, S. J. Limmer, Y. Wang, and G. Cao, *Growth and electrochemical properties of single-crystalline V2O5 nanorod arrays*, Jap. J. Appl. Phys. **44**, 662 (2005).
30. Y. Wang, Z. Li, X. Sheng, and Z. Zhang, *Synthesis and optical properties of V_2O_5 nanorods*, J. Chem. Phys. **126**, 164701 (2007).
31. M. E. Spahr, P. Bitterli, R. Nesper, M.M¨uller, F. Krumeich, and H. U. Nissen, *Redox active nanotubes of vanadium oxide*, Angew. Chem. Int. Ed. **37**, 1263 (1998).
32. S. Shin, B.H. Kong, B.S. Kim, K.M. Kim, H.K. Cho, and H.H. Cho, *Over 95% of large-scale length uniformity in template-assisted electrodeposited nanowires by sub-zero-temperature electro deposition*, Nanoscale Res. Lett. **6**, 467 (2011).
33. L. Mai, W. Guo, B. Hu, W. Jin, and W. Chen, *Fabrication and properties of VOx –based nanorods*, J. Phys. Chem. C **112**, 423 (2008).
34. C.W. Zou, and W. Gao, Fabrica*tion, optoelectronic and photo catalytic properties of some composite oxide nanostructures*, Trans. Electr. Electron. Mater. **11**, 1 (2010).
35. K. Jeyalakshmi, K.K. Purushothaman, and G. Muralidharan, *Thickness dependent supercapacitor behaviour of sol-gel spin coated nanostructured vanadium pentoxide thin films*, Philos. Mag. **93**, 1490 (2013).
36. M. Benmoussa, A. Outzourhit, A. Bennouna, and A. Ihlal, *Li^+ ions diffusion into sol-gel V_2O_5 thin films: electrochromic properties*, Eur. Phys. J. Appl. Phys. **48**, 10502 (2009).

37. M. Benmoussa, A. Outzourhit, R. Jourdani, A. Bennouna, E.L. Ameziane, *Structural, optical and electrochromic properties of sol-gel V_2O_5 thin films*, Active and Passive Elec. Comp. **26**, 245 (2003).
38. D. Liu, Y. Liu, B. Batalla Garcia, Q. Zhang, A. Pan, Y. H. Jeong, and G. Cao, *V_2O_5 xerogel electrodes with much enhanced lithium-ion intercalation properties with N_2 annealing*, J. Mater. Chem. **19**, 8789 (2009).
39. Z. Wang, J. Chen, and X. Hu, *Electrochromic properties of aqueous sol-gel derived vanadium oxide films with different thickness*, Thin Solid Films **375**, 238 (2000).
40. S. Kim, G. Nam, H. Yoon, H. Park, H. Choi, J.S. Kim, J.S. Kim, D.Y. Kim, S.-O. Kim, and J.-Y.Leem*, Structural, optical, and electrical properties of ZnO thin films deposited by sol-gel dip-coating process at low temperature*, Electron. Mater. Lett. **10**, 869 (2014).
41. Mohammed Alsawafta, Afaf Almoabadi, Simona Badilescu and Vo-Van Truong, *Improved Electrochromic Properties of vanadium Pentoxide Nanorods Prepared by Thermal Treatment of Sol-Gel Dip-Coated Thin Films*, J. Electrochem. Soc. **162**, H466 (2015).
42. C.-L.Wu, C.-K.Wang, C.-K.Lin, S.-C.Wang, and J.-L. Huang, *Electrochromic properties of nanostructured tungsten oxide films prepared by surfactant-assisted sol-gel process*, Surf. Coat. Technol. **231**, 403 (2013).
43. S. Badilescu, and P. V. Ashrit, *Study of sol-gel prepared nanostructured WO_3 thin films and composites for electrochromic applications*, Solid State Ionics **158**, 187 (2003).
44. M. Sadakane, K. Sasaki, H. Kunioku, B. Ohtani, R. Abe, and W. Ueda, *Preparation of 3-D ordered macroporous tungsten oxide using a colloidal crystal template method, and their structural characterizaon and application as photocatalysts under visible light irradiation*, J. Mater. Chem. **20**, 1811 (2010).
45. E. Bica, E. J. Popovici, M. Stefan, I. Perhaita, L. Barbu-Tudoran, E. Indrea, and I. C. Popescu, *Morphological, structural and optical characterization of tungsten trioxide films prepared by sol-gel route: effect of substrate and annealing temperature*, Dig. J. Nanomater. Biostruct. **6**, 1935 (2011).
46. D. Nagao, R. Kameyama, H.Matsumoto, Y. Kobayashi, and M. Konno, *Single- and multi-layered patterns of polystyrene amd silica particles assembled with a simple dip-coating*, Colloids and Surfaces A: Physicochem. Eng. Aspects **317**, 722 (2008).

47. C. C. Chen, *Characterization of porous WO_3 electrochromic device by electrochemical impedance spectroscopy*, Journal of Nanomaterials **2013**, Article ID 785023 (2013).
48. D. S. Raimundo, F. J. R. Fernandez, and W. J. Salcedo, J. Integrated Circuits and Systems **1**, 39 (2006).
49. O. D. Velev, and A. M. Lenhoff, *Colloidal crystals as templates for porous materials*, Curr. Opin. Colloid. Interface Sci. **5**, 56 (2000).
50. Q. B. Meng, Z.-Z.Gu, and O. Sato, *Fabrication of Highly Ordered Porous Structures*, Appl. Phys. Lett. **77**, 4313 (2000).
51. M. Deepa, A. K. Srivastava, S. N. Sharma, and S. M. Shivaprasad, *Microstructural and electrochromic properties of tungsten oxide thin films produced by surfactant-mediated electrodeposition*, Appl. Surf. Sci. **254**, 2342 (2008).
52. N. Özer,*Electrochemical properties of sol-gel deposited vanadium pentoxide films*, Thin Solid Films **305**, 80 (1997).
53. S.M.Attia, Jue WANG, Guanqming WU, Jun SHEN, and Jianhua MA, *Review on Sol-Gel Derived Coatings: Process, Techniques and optical Application*, J. Mater. Sci. Technol. **18**, 211 (2002).
54. K D Vernon-Parry, *Scanning Electron Microscopy: an introduction*, Elsevier **13**, 40 (2000).
55. G.D. Gilliland, *Photoluminescence spectroscopy of crystalline semiconductors,* Mater. Sci. Eng., R **18**, 99 (1997).
56. Peter T. Kissinger, and William R. Heineman, *Cyclic Voltammetry*, Journal of Chemical Education **60**, 702 (1983).
57. M. Kang, S. W. Kim, J.-W. Ryu, Y. Xu, and R. Kato*, Optical and Thermal Properties of V_2O_5 Thin Films with Crystallization*, J. Korean Phys. Soc. **62**,1134 (2013).
58. M. Balters, K. Cassiers, and P. Van der Voort, P. M.Weckhuisen, R. A. Schoonheydt, and E. F. Vansant, *MCM-48-Supported Vanadium Oxide Catalysts, Prepared by the Molecular Designed Dispersion of VO(acac)2: A Detailed Study of the Highly Reactive MCM-48 Surface and the Structure and Activity of the Deposited VOx*, J. Catal. **197**, 160 (2001).
59. C. Julien, G. A. Nazri, and O. Bergstrom, *Raman Scattering Studies of Microcrystalline V6O13*, Phys. Stat. Solidi B **20**, 319 (1997).

60. W. Chen, L.Mai, J. Peng, Q. Xu, and Q. Zhu, *Raman spectroscopic study of vanadium oxide nanotubes*, J. Solid State Chem. **177**, 377 (2004).

61. H. K. Koduru, H. M. Obili, and G. Cecilia, *Spectroscopic and electrochromic properties of activated reactive evaporated nano-crystalline V_2O_5 thin films grown on lexible substrates*, Int. Nano Lett. **3**, 24 (2013).

62. R. Cecatto, S. Dire, T. Barone, G. De Santo, and E. Cazzanelli, *Growth of nanotubes in sol-gel-derived V_2O_5 powders and films prepared under acidic conditions*, J. Mater Res. **24**, 475 (2009).

63. N. Thi Be Bay, P. Minh Tien, S. Badilescu, Y. Djaoued, G. Bader, F. E. Girouard, V. V. Truong, and Q. Le, *Nguyen Optical and electrochemical properties of vanadium pentoxide gel thin films*, J. Appl. Phys. **80,** 7041 (1996).

64. Z. Tong, J. Hao, K. Zhang, J. Zhao, B-L. Su, and Y. Li, *Improved electrochromic performance and lithium diffusion coefficient in three-dimensionally ordered macro porous V_2O_5 films*, J. Mater. Chem C. **2,** 3651 (2014).

65. P. Liu, S. H. Lee, C. E. Edwin Tracy, J. A. Turner, J. R. Pitts, and S. K Deb, *Electrochromic and chemochromic performance of mesoporous thin-film vanadium oxide*, Solid State Ionics **165,** 223 (2003).

66. D. Sun, C. W. Kwon, G. Baure, E. Richman, J. MacLean, B. Dunn, and S. H. Tolbert, *The Relationship Between Nanoscale Structure and Electrochemical Properties of Vanadium Oxide Nanorolls*, Adv. Funct. Mater. **14**, 1197 (2004).

67. A. Jin, W. Chen, Q. Zhu, Y. Yang, V.L. Volkov, and G.S. Zakharova, *Electrical and electrochemical characterization of poly(ethylene oxide)/V_2O_5 xerogel electrochromic films*, Solid State Ionics **179**, 1256 (2008).

68. Y. Zhang, Y. Liu, Y. Cheng, and X. Hu, *Electrochemical impedance spectra of V_2O_5 xerogel films with intercalation of lithium ion*, J. Cent. South Univ. Technol. **12**, 309 (2005).